



## Supporting Information

### **Double-Exchange-Induced *in situ* Conductivity in Nickel-Based Oxyhydroxides: An Effective Descriptor for Electrocatalytic Oxygen Evolution**

*Bailin Tian<sup>+</sup>, Hyeyoung Shin<sup>+</sup>, Shengtang Liu, Muchun Fei, Zhangyan Mu, Cheng Liu, Yanghang Pan, Yamei Sun, William A. Goddard III,\* and Mengning Ding\**

[anie\\_202101906\\_sm\\_miscellaneous\\_information.pdf](#)

# Supporting Information

---

## Contents

Experimental Methods .....	2
Characterization of Electrocatalysts.....	5
Standard Crystal Structures .....	13
Device Fabrication Procedures .....	14
Evidences for the Hydroxides Formation after CV Activations .....	19
Exclude the Influence of Oxygen Vacancies and Morphology .....	22
Bulk OER Electrochemical Test of the Catalysts .....	23
Separated CV & ETS results of Electrocatalysts with DE Interaction .....	24
Comparisons of $iR$ & $\Delta\eta$ at Sequential Integral Current Densities .....	27
Systematic Mechanism Investigation of other NiFe Hydroxides .....	28
Stability Test of $\alpha^*$ - $\text{Ni}_{0.9}\text{Ir}_{0.1}$ Catalyst.....	29
Post-OER XRD Patterns and XPS Spectra.....	30
Illustration of Possible DE interactions for $\alpha^*$ - $\text{Ni}_{0.9}\text{Ru}_{0.1}$ Catalyst.....	32
Illustration of Catalysts cannot undergo DE interactions .....	33
pH Dependent CV & ETS Experiments .....	35
Additional pDOS of other OER Intermediates .....	36
Atomic Coordinates for All States in Figure 1a State 1 .....	39
Atomic Coordinates for All States in Figure 1b (Fe) State 1 .....	46
Supplementary References .....	53

## Experimental Methods

**Chemicals.** All chemical reagents were used as received without further purification.

**Synthesis of Nano-electrocatalysts.** The  $\alpha\text{-Ni(OH)}_2$  was prepared through an alcohothermal method.<sup>[1]</sup> In a typical procedure,  $\text{Ni}(\text{NO}_3)_2 \cdot 6\text{H}_2\text{O}$  (1 mmol) was dissolved in ethanol (20 mL), followed by quick addition of oleylamine (2 mL) and ethanol (10 mL). The mixture was stirred for 0.5 h to produce a homogeneous solution, which was then transferred into a 50 mL Teflon-lined autoclave. The autoclave was sealed and maintained at 180 °C for 15 h in a convection oven and then allowed to cooled naturally to room temperature. The resulting green precipitant was collected and washed with cyclohexane, ethanol, and distilled water several times and was then dried under vacuum at 60 °C for 6 h. To prepare  $\beta\text{-Ni(OH)}_2$  hexagonal nanoplates, we used the same procedure as for  $\alpha\text{-Ni(OH)}_2$  except that the 20 mL of ethanol was replaced by 20 mL of deionized (DI) water (milli-Q filtered, 18.2 MΩ·cm). To prepare  $\alpha\text{-Ni(OH)}_2$  doped with various elements, we used the same synthetic procedure as for  $\alpha\text{-Ni(OH)}_2$  except that the 1 mmol of  $\text{Ni}(\text{NO}_3)_2 \cdot 6\text{H}_2\text{O}$  was replaced by 0.9 mmol of  $\text{Ni}^{2+}$  ( $\text{Ni}(\text{NO}_3)_2 \cdot 6\text{H}_2\text{O}$  or  $\text{NiCl}_2 \cdot 6\text{H}_2\text{O}$ ) + 0.1 mmol of doped metal ions. To prepare various doped  $\beta\text{-Ni(OH)}_2$  materials, we used the same synthesis procedure for  $\beta\text{-Ni(OH)}_2$  hexagonal nanoplates except that the 1 mmol of  $\text{Ni}(\text{NO}_3)_2 \cdot 6\text{H}_2\text{O}$  was replaced by 0.9 mmol of  $\text{Ni}^{2+}$  ( $\text{Ni}(\text{NO}_3)_2 \cdot 6\text{H}_2\text{O}$  or  $\text{NiCl}_2 \cdot 6\text{H}_2\text{O}$ ) + 0.1 mmol of doped metal salts. Anions used in two inorganic salts were kept the same.

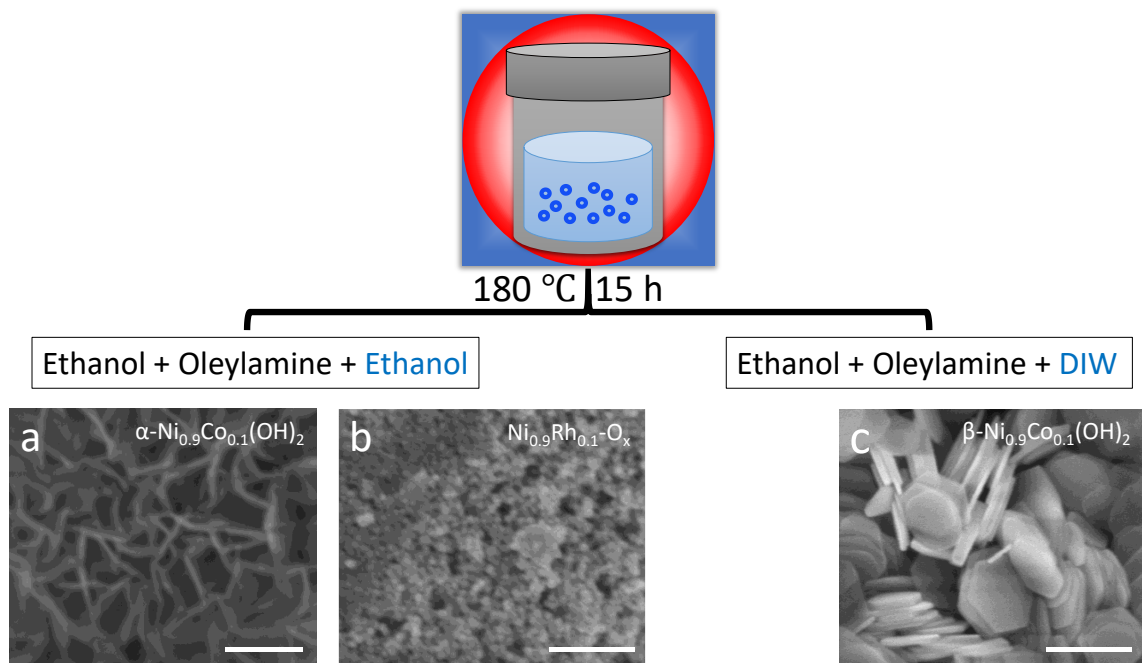


**Figure S1.** Scanning electron microscopy (SEM) images of the prepared nanosheet assembled  $\alpha\text{-Ni}_{0.9}\text{Co}_{0.1}(\text{OH})_2$  (a), face-centered cubic (fcc) nickel alloys with surface oxides (b), and  $\beta\text{-Ni}_{0.9}\text{Co}_{0.1}(\text{OH})_2$  hexagonal nanoplates (c) by a facile solvothermal method, scale bars are 250 nm in a-c.

**Fabrication of the hydroxide devices.** A free standing film was assembled from as-prepared Ni-based hydroxides suspension by a co-solvent evaporation method.<sup>[2]</sup> Typically, Ni-based hydroxide suspensions in ethanol (4 mL,  $\sim 5\text{ mg}\cdot\text{mL}^{-1}$ ) were mixed with DI water (milli-Q filtered, 6 mL) and n-butanol (2.5 mL). The suspension of Ni-based hydroxides in mixed solvents was added drop by drop into a flask (about 9 cm

in diameter) filled with DI water. A film of Ni-based hydroxides was then formed on the water surface and later transferred onto the device. In specific, a PMMA (A8, MicroChem Corp.) film was prepared by spin coating on the substrate (p++ silicon wafer with 300 nm thermal oxide) surface with pre-patterned Ti/Au electrodes (20/50 nm). E-beam lithography (EBL) was then used to open windows on PMMA with desired patterns. The as-prepared free-standing films of Ni-based hydroxides were then transferred to the substrate surface. After the removal of PMMA template, Ni-based hydroxides films were deposited on the device with desired patterns. To eliminate the influence of electrolyte and to avoid electrochemical reactions on the metal electrodes, another layer of PMMA (can be adjusted by coating times, electrochemically inert) was then deposited on the device with hydroxide film patterns and a smaller window that only exposes hydroxides was opened by EBL. In this work all the electrochemical windows were set to  $20\text{ }\mu\text{m} \times 30\text{ }\mu\text{m}$  for current density and sheet conductance normalization. The final device, with exposed Ni-based hydroxides and insulated electrodes was used for on-chip electrochemistry and *in situ* electrical transport spectroscopy (ETS) measurements.

**On-chip CV and *in situ* electrical transport (ETS) measurements.** A two channel (Source/Measure Unit) SMU (Agilent B2902a) was used for the measurements. The first SMU channel was used as a potentiostat to control the potential of source electrode as to the reference electrode ( $V_G$ ), while collecting the current ( $I_G$ ) through the counter electrode. A leak-free Ag/AgCl (Harvard Apparatus LF-2) electrode and a platinum wire were used as reference and counter electrode, respectively. In a typical CV measurement, the scan rate is  $2\text{ mV}\cdot\text{s}^{-1}$ . The oxygen evolution reaction activity (OER) was evaluated in 1M KOH (99.999%, electronic grade) aqueous electrolyte. The measured potential vs.  $E_{\text{Ag}/\text{AgCl}}$  was converted to reverse hydrogen electrode potential (RHE). The measured potential vs.  $E_{\text{Ag}/\text{AgCl}}$  (of LF-2) was converted to reverse hydrogen electrode potential (RHE) based on the Nernst equation,  $V_{\text{RHE}} = E_{\text{vs. Ag/AgCl}} + 0.059\text{pH} + E^0$ , where  $E^0 = 0.2046\text{ V}$  at  $298.15\text{ K}$ . The second SMU was used to supply a small bias voltage (50 mV) between drain and source electrodes and collecting the corresponding lateral transport current ( $I_{\text{DS}}$ ). For a typical measurement in this study, the Gate (Faradaic) current ( $I_G$ ) is generally smaller than the  $I_{\text{DS}}$  current (by up to three orders of magnitude). When the electrochemical current  $I_G$  is significant enough to affect the accuracy of  $I_{\text{DS}}$ , the presented equivalent circuit (Fig. S18) can be used to subtract the  $I_G$  background from the ETS ( $I_{\text{DS}}$ ) channel.

**Electrical conductivity calculations.** The *in situ* sheet conductance and electrical conductivity were calculated by

$$G_s = \frac{I_{\text{cond}} \cdot l}{V_{\text{DS}} \cdot w}$$

$$\sigma = \frac{I_{\text{cond}} \cdot l}{V_{\text{DS}} \cdot w \cdot h}$$

where  $I_{\text{cond}}$  is the conductive current (equals to  $I_2$  in Fig. S18),  $l$  is the length of electrochemical window (typically  $30\text{ }\mu\text{m}$ ),  $w$  is the width of electrochemical window (typically  $20\text{ }\mu\text{m}$ ),  $V_{\text{DS}}$  is the small bias voltage (50 mV) between drain and source electrodes, and  $h$  is the average film thickness determined by AFM.

**Bulk electrochemical measurements.** Typically, 5 mg of catalyst was dispersed in ethanol (640  $\mu\text{L}$ ), DI water (18.2  $\text{M}\Omega\cdot\text{cm}$ , 320  $\mu\text{L}$ ) and Nafion solution (5 wt% in ethanol, 40  $\mu\text{L}$ ) to form a well dispersed ink. For fabrication of the working electrode, 50  $\mu\text{L}$  of

the catalyst ink was dropped onto 1 cm<sup>2</sup> carbon paper. The electrode was then dried at room temperature. The mass loading of the catalyst was 0.25 mg·cm<sup>-2</sup>.

Electrochemical experiments were performed in a typical three-electrode system using a potentiostat (CS3004, CorrTest Instruments). All electrochemical cell components were cleaned prior to experiments with 0.5 M H<sub>2</sub>SO<sub>4</sub> and rinsed with DI H<sub>2</sub>O (18.2 MΩ·cm). Before the electrochemical measurement, the electrolyte was degassed by bubbling oxygen for at least 30 min to achieve a saturation condition of oxygen gas. All potentials were referenced to a Hg/HgO reference electrode, and platinum wire was used as the counter electrode in all measurements. The measured potential vs. E<sub>Hg/HgO</sub> was converted to reverse hydrogen electrode potential (RHE) based on the Nernst equation,  $V_{\text{RHE}} = E_{\text{vs. Hg/HgO}} + 0.059 \times \text{pH} + E^{\circ}$ , where  $E^{\circ} = 0.098$  V at 298.15 K. All electrochemical was presented without IR-correction. Cyclic voltammetry (CV) measurements set 5 mV·s<sup>-1</sup>.

**Density functional theory (DFT) simulations.** Spin-polarized density functional theory calculations with the choice of Perdew–Burke–Ernzerhof (PBE) exchange-correlation functional<sup>[3]</sup> were performed using the Vienna Ab-initio Simulation Package (VASP).<sup>[4]</sup> The projector augmented wave (PAW) method<sup>[5]</sup> was employed to describe the interaction between valence electrons and ions. We set the plane-wave energy cutoff to 400 eV and we used the  $\Gamma$ -centered (3×3×1) Monkhorst–Pack K-point grids. All calculations were carried out with the periodic γ-NiOOH (100) based slab models as in our previous studies.<sup>11</sup> In addition, the Poisson–Boltzmann (PB) implicit solvation model was employed to include solvation.

**Materials Characterization.** The as-synthesized samples were examined by X-ray powder diffraction (XRD), which was carried out on a Shimadzu Lab X/XRD-6000 X-ray diffractometer equipped with a Cu-Kα radiation source ( $\lambda = 1.5418$  Å) operating at 40 kV and 30 mA. Scanning electron microscope (SEM) images were recorded on Hitachi S-4800 with samples deposited on carbon conductive tapes. X-ray photoelectron spectroscopy (XPS) was performed on a UIVAC-PHI 5000 Versa Probe spectrometer with Al Kα as radiation source. The binding energies in recorded spectra were calibrated by the C 1s peak, the internal standard reference at 284.6 eV. The thickness of on-chip devices was measured with Atomic Force microscope (Bruker Dimension Icon). Raman spectroscopy was tested on HORIBA XploRA PLUS Raman microscope with laser wavelength of 532 nm.

## Characterization of Electrocatalysts

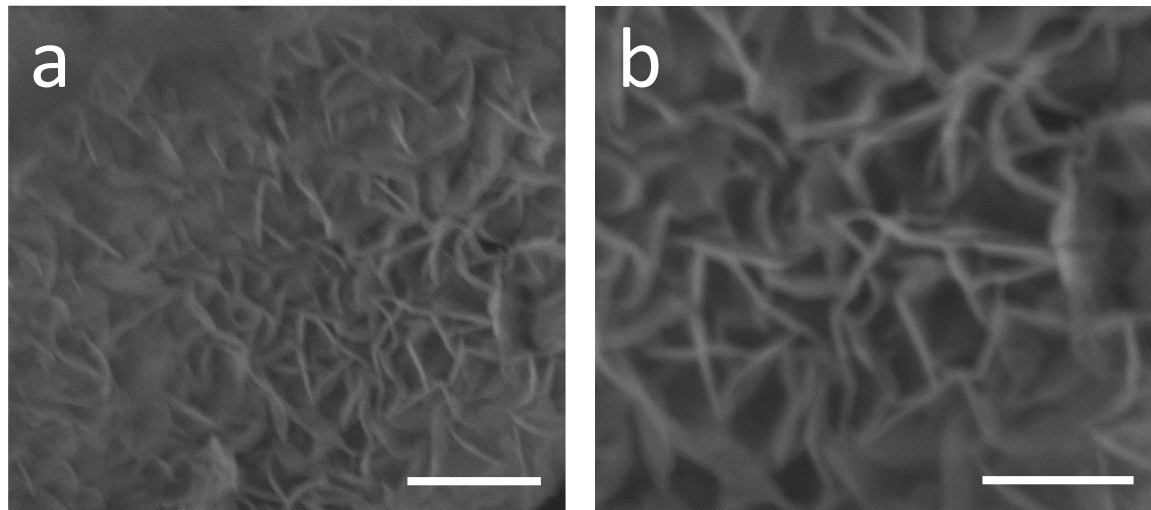


**Figure S2.** SEM images of the representative nanosheet assembled  $\alpha\text{-Ni}_{0.9}\text{Co}_{0.1}(\text{OH})_2$  (**a, b**), scale bars are 500 nm and 250 nm, respectively.

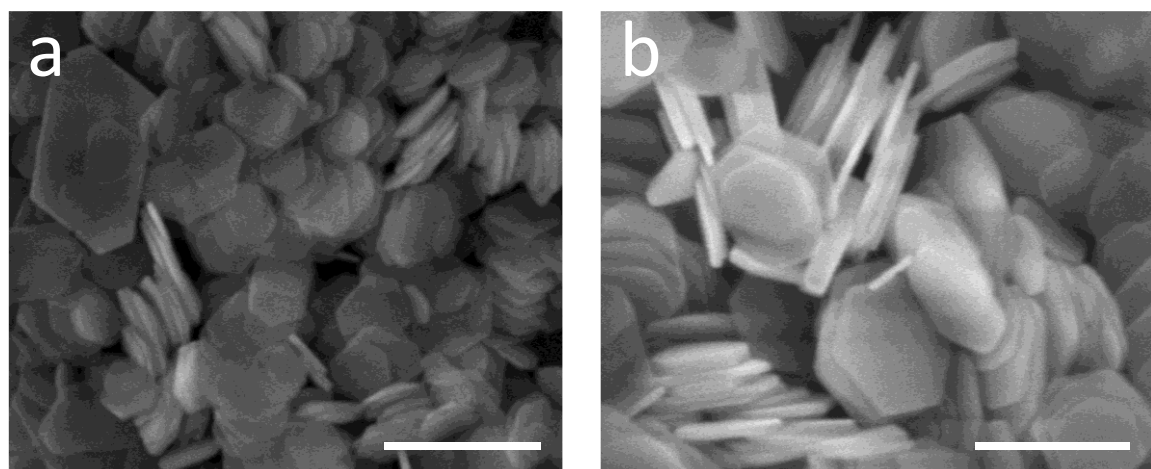


**Figure S3.** SEM images of the representative  $\beta\text{-Ni}_{0.9}\text{Co}_{0.1}(\text{OH})_2$  nanoplates (**a, b**), scale bars are 500 nm and 250 nm, respectively.

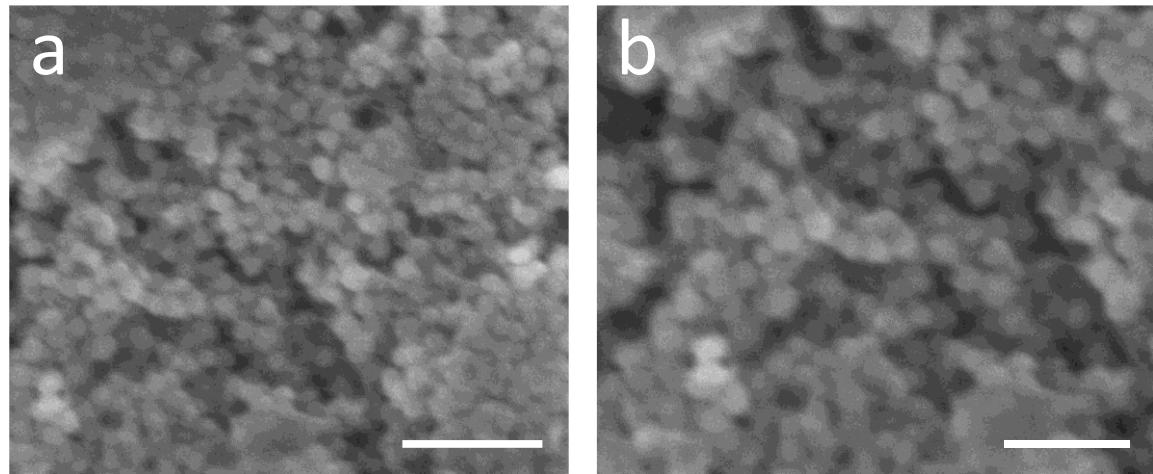


**Figure S4.** SEM images of the representative fcc  $\text{Ni}_{0.9}\text{Rh}_{0.1}\text{-O}_x$  nanoparticles (**a, b**), scale bars are 150 nm and 100 nm, respectively.

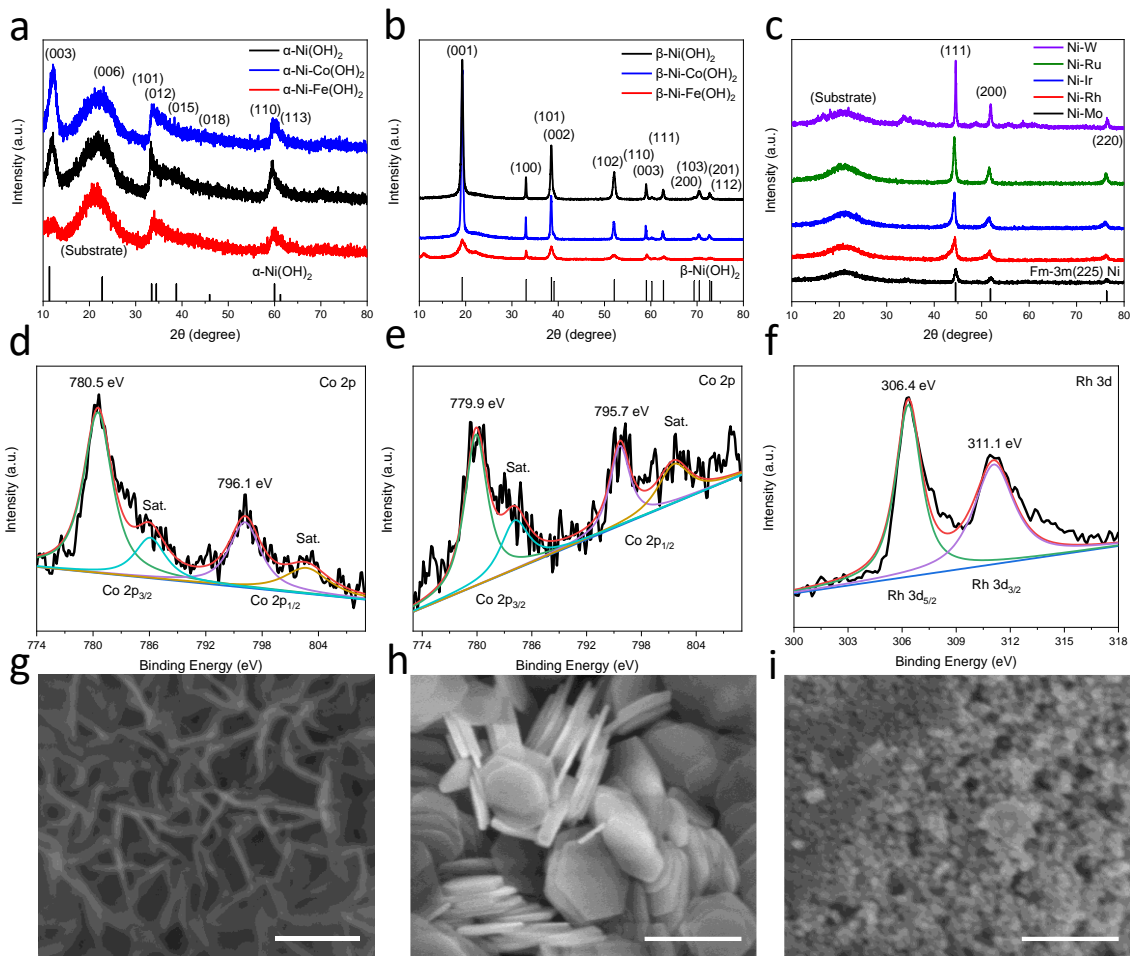


**Figure S5.** Material characterizations. (a) XRD patterns of pure hexagonal  $\alpha\text{-Ni(OH)}_2$  (JCPDS 380715) and doped  $\alpha\text{-Ni(OH)}_2$ . (b) XRD patterns of pure hexagonal  $\beta\text{-Ni(OH)}_2$  (JCPDS 140117) and doped  $\beta\text{-Ni(OH)}_2$ . (c) XRD patterns of face-centered cubic (fcc) nickel alloys (JCPDS 040850). (d) Pristine state XPS spectrum of Co 2p for  $\alpha\text{-Ni}_{0.9}\text{Co}_{0.1}(\text{OH})_2$ . (e) Pristine state XPS spectrum of Co 2p for  $\beta\text{-Ni}_{0.9}\text{Co}_{0.1}(\text{OH})_2$  nanoplates. (f) Pristine state XPS spectrum of Rh 3d for  $\text{Ni}_{0.9}\text{Rh}_{0.1}\text{-O}_x$  nanoparticles. Black curves depict the original XPS spectra and colored curves represent the fitted peaks. The SEM image of representative hexagonal nanosheets assembled  $\alpha\text{-Ni}_{0.9}\text{Co}_{0.1}(\text{OH})_2$  (g), hexagonal  $\beta\text{-Ni}_{0.9}\text{Co}_{0.1}(\text{OH})_2$  nanoplates (h) and  $\text{Ni}_{0.9}\text{Rh}_{0.1}\text{-O}_x$  nanoparticles (i). Scale bars are 250 nm in g-i.

The main peak of Co 2p<sub>3/2</sub> at 780.2 eV and 2p<sub>1/2</sub> peak at 796.0 eV were assigned to Co<sup>2+</sup>. It seems that the valence state of Co ions in  $\alpha\text{-Ni}_{0.9}\text{Co}_{0.1}(\text{OH})_2$  is a little higher than that in  $\beta\text{-Ni}_{0.9}\text{Co}_{0.1}(\text{OH})_2$ . Moreover, the Rh 3d peaks at 306.4 eV and 311.1 eV were assigned to Rh species.

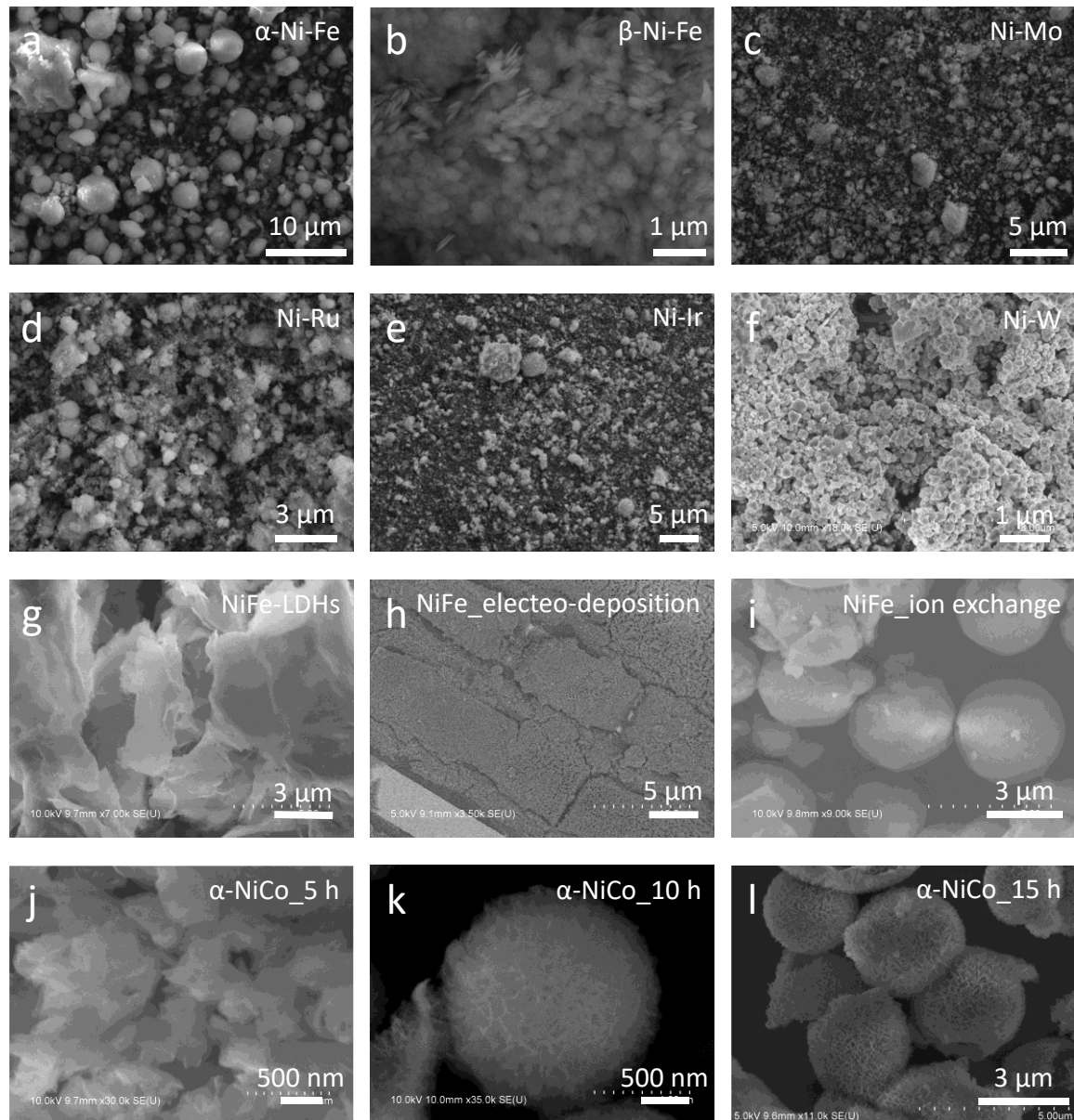


**Figure S6.** The SEM images of other catalysts.

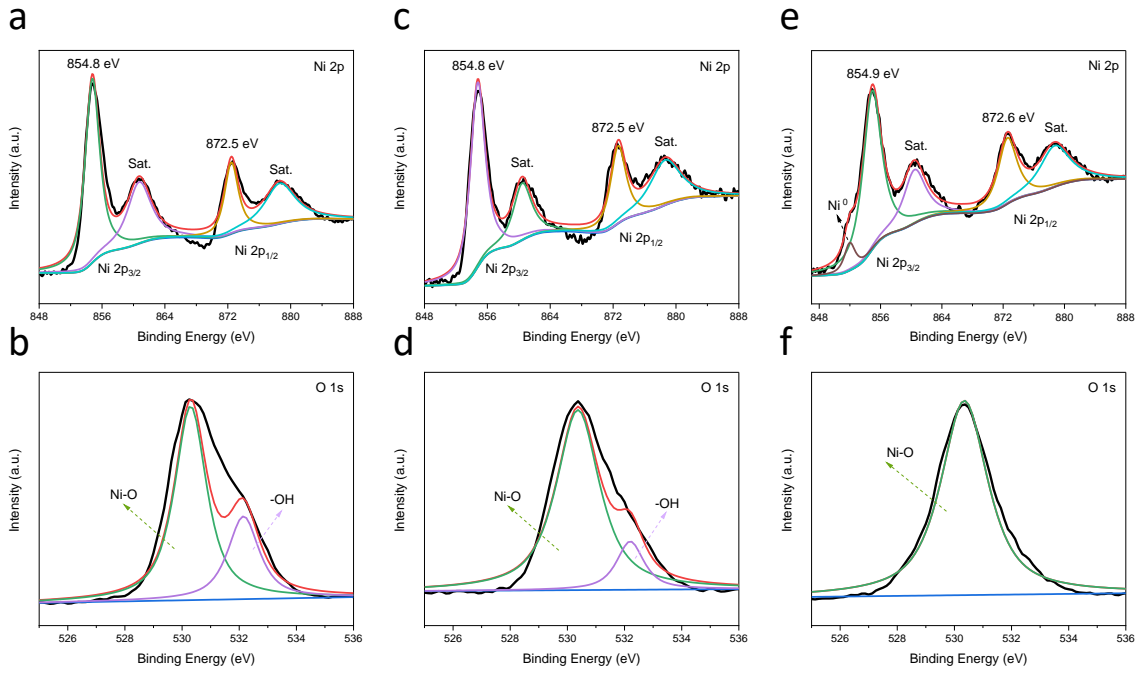


**Figure S7.** Pristine state XPS spectra of Ni 2p (**a**) and O 1s (**b**) in  $\alpha\text{-Ni}_{0.9}\text{Co}_{0.1}(\text{OH})_2$ . Pristine state XPS spectra of Ni 2p (**c**) and O 1s (**d**) in  $\beta\text{-Ni}_{0.9}\text{Co}_{0.1}(\text{OH})_2$  nanoplates. Pristine state XPS spectra of Ni 2p (**e**) and O 1s (**f**) in  $\text{Ni}_{0.9}\text{Rh}_{0.1}\text{-O}_x$  nanoparticles. Black curves depict the original XPS spectra and colored curves represent the fitted peaks. The main peak of  $\text{Ni}^{2+}$  at 854.8 eV and  $2p_{1/2}$  peak at 872.5 eV shown the valence states of Ni in the surface of three kinds of electrocatalysts were about +2.<sup>[6]</sup>

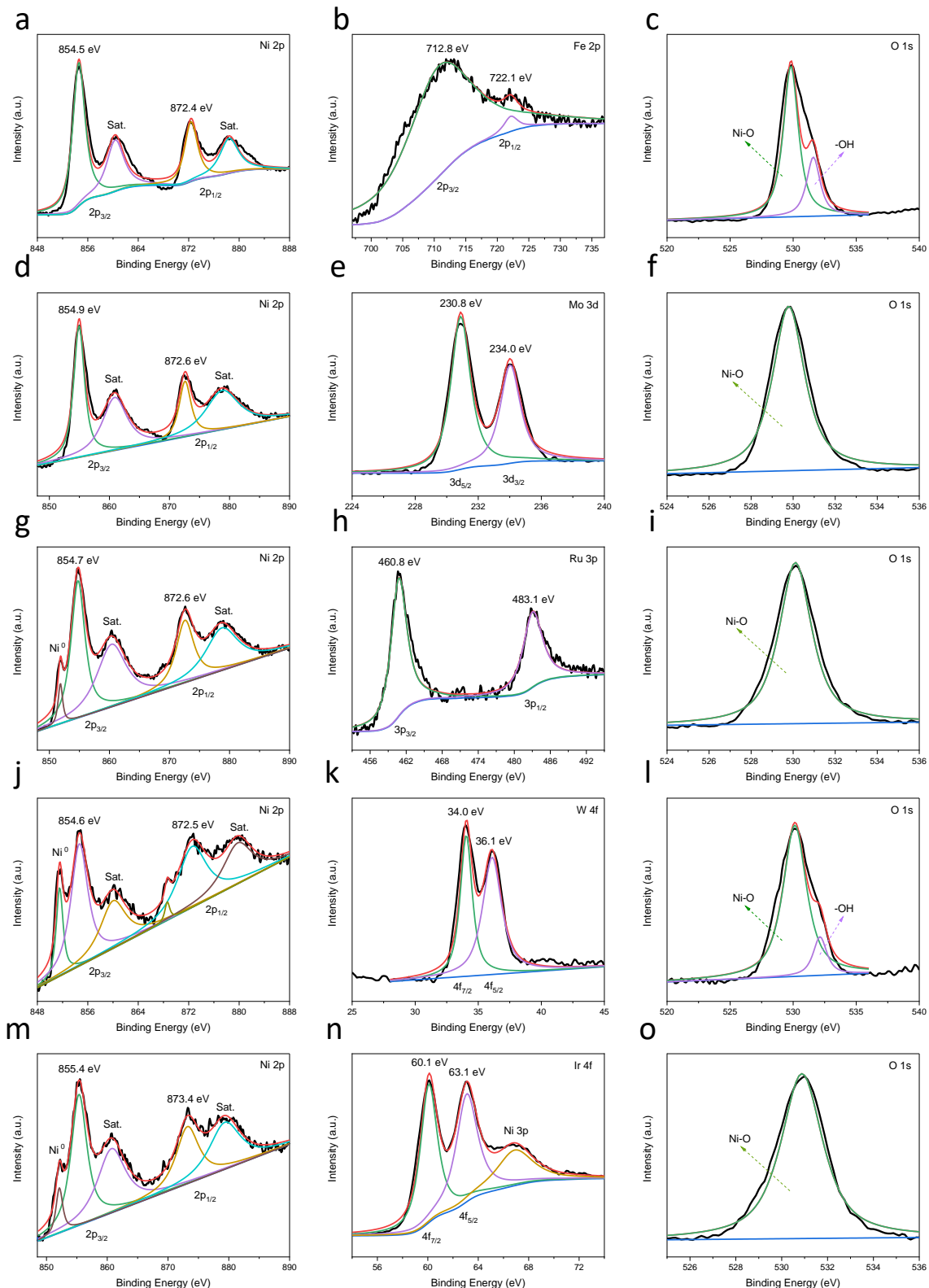


**Figure S8.** The pristine state XPS spectra of Ni 2p, Fe 2p, O 1s in  $\alpha$ -Ni<sub>0.9</sub>Fe<sub>0.1</sub>(OH)<sub>2</sub> (**a-c**). The pristine state XPS spectra of Ni 2p, Mo 3d, O 1s in Ni<sub>0.9</sub>Mo<sub>0.1</sub>-O<sub>x</sub> (**d-f**). The pristine state XPS spectra of Ni 2p, Ru 3p, O 1s in Ni<sub>0.9</sub>Ru<sub>0.1</sub>-O<sub>x</sub> (**g-i**). The pristine state XPS spectra of Ni 2p, W 4f, O 1s in Ni<sub>0.9</sub>W<sub>0.1</sub>-O<sub>x</sub> (**j-l**). The pristine state XPS spectra of Ni 2p, Ir 4f, O 1s in Ni<sub>0.9</sub>Ir<sub>0.1</sub>-O<sub>x</sub> (**m-o**). Black curves depict the original XPS spectra and colored curves represent the fitted peaks. The XPS spectra indicated the successful synthesis of different metal elements doped electrocatalysts.

The binding energy of Ni 2p and Fe 2p peaks in pristine  $\alpha\text{-Ni}_{0.9}\text{Fe}_{0.1}(\text{OH})_2$  indicated the valence states of Ni and Fe were around +2 and +3, respectively. The binding energy of Ni 2p and Mo 3d peaks in pristine  $\text{Ni}_{0.9}\text{Mo}_{0.1}\text{-O}_x$  indicated the valence states of Ni and Mo were around +2 and +4, respectively. The binding energy of Ni 2p and Ru 3p peaks in pristine  $\text{Ni}_{0.9}\text{Ru}_{0.1}\text{-O}_x$  indicated the valence states of Ni and Ru were around (+0) +2 and +0, respectively. The binding energy of Ni 2p and W 4f peaks in pristine  $\text{Ni}_{0.9}\text{W}_{0.1}\text{-O}_x$  indicated the valence states of Ni and W were around (+0) +2 and +4, respectively. The binding energy of Ni 2p and Ir 4f peaks in pristine  $\text{Ni}_{0.9}\text{Ir}_{0.1}\text{-O}_x$  indicated the valence states of Ni and Ir were around (+0) +2 and +0, respectively. The attribution of all the peaks is based on the standard database (<https://srdata.nist.gov/xps/Default.aspx>).

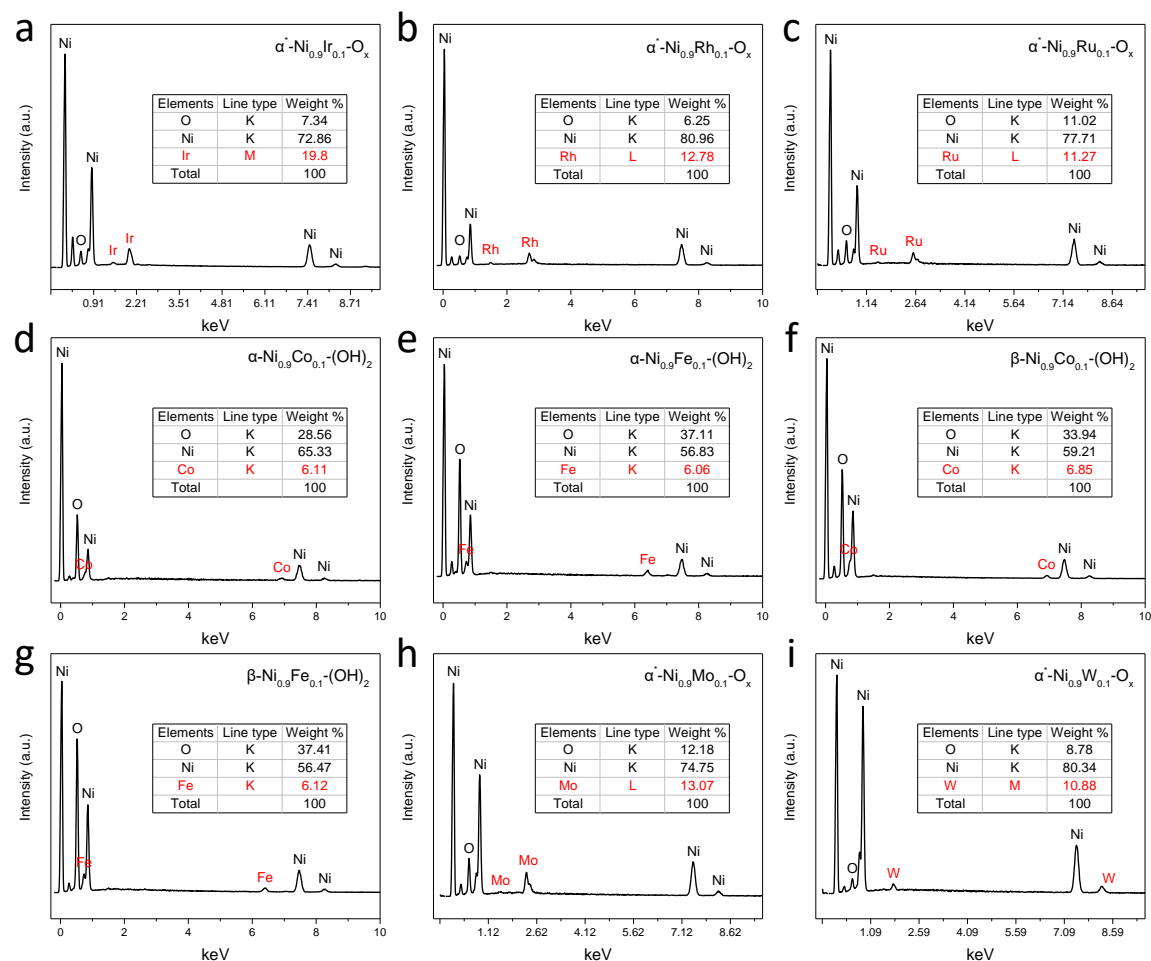


**Figure S9.** EDS analysis of Ni-based catalysts with various dopants (Ir, Ru, Rh, Co, Mo, Fe and W). Molar ratio (converted from weight percentage) show that all of the doping levels are around  $10\% \pm 1.5\%$ , except for the W doped sample (probably due to the low solubility of  $\text{WCl}_6$  in ethanol during synthesis).

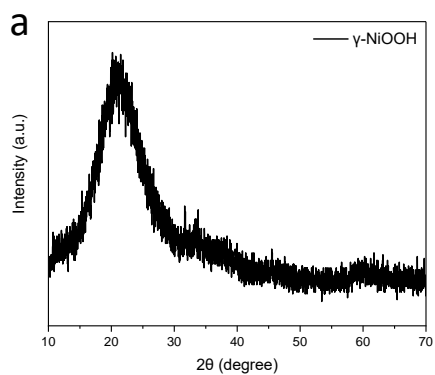


**Figure S10.** XRD pattern of  $\gamma$ -NiOOH nanoparticles (a), which revealed no evidence for a clearly crystalline phase.<sup>[7]</sup>

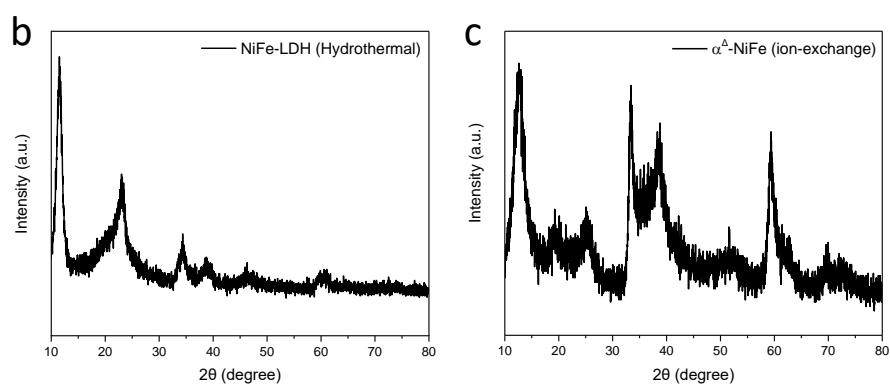


**Figure S11.** XRD pattern of NiFe-LDH (hydrothermal)<sup>[8]</sup> (b), and XRD pattern of  $\alpha^{\Delta}$ -NiFe (ion-exchange)<sup>[9]</sup> (c).

## Standard Crystal Structures

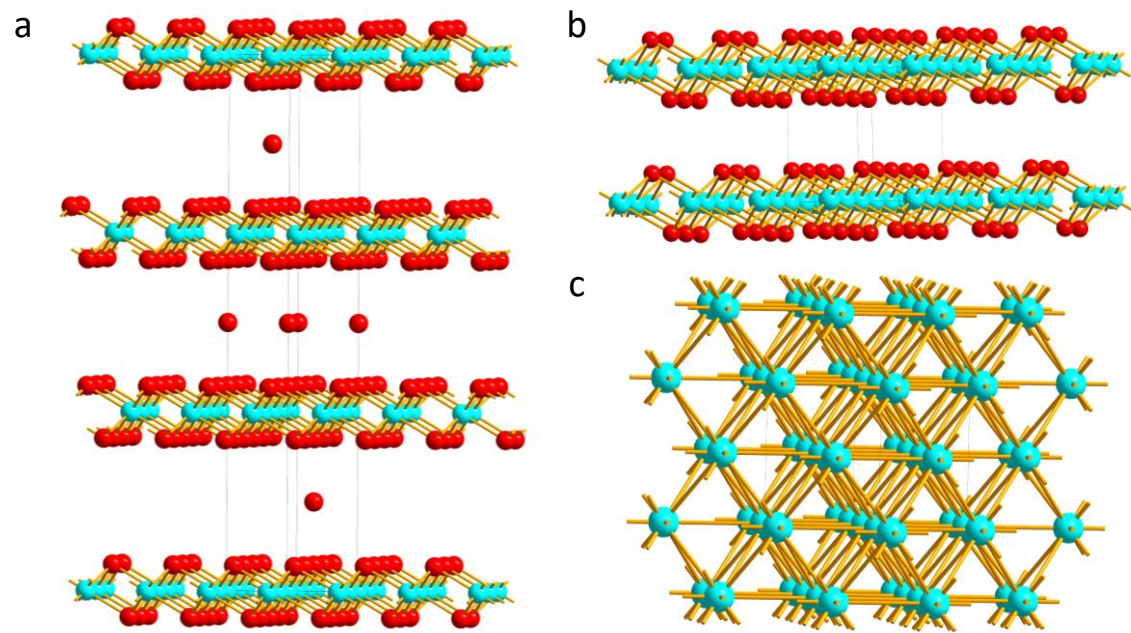


**Figure S12.** Standard crystal structures for  $\alpha\text{-Ni(OH)}_2$  (a),  $\beta\text{-Ni(OH)}_2$  (b) and fcc Nickel (c). The cyan and red ball represent Ni and O atoms, respectively.

## Device Fabrication Procedures

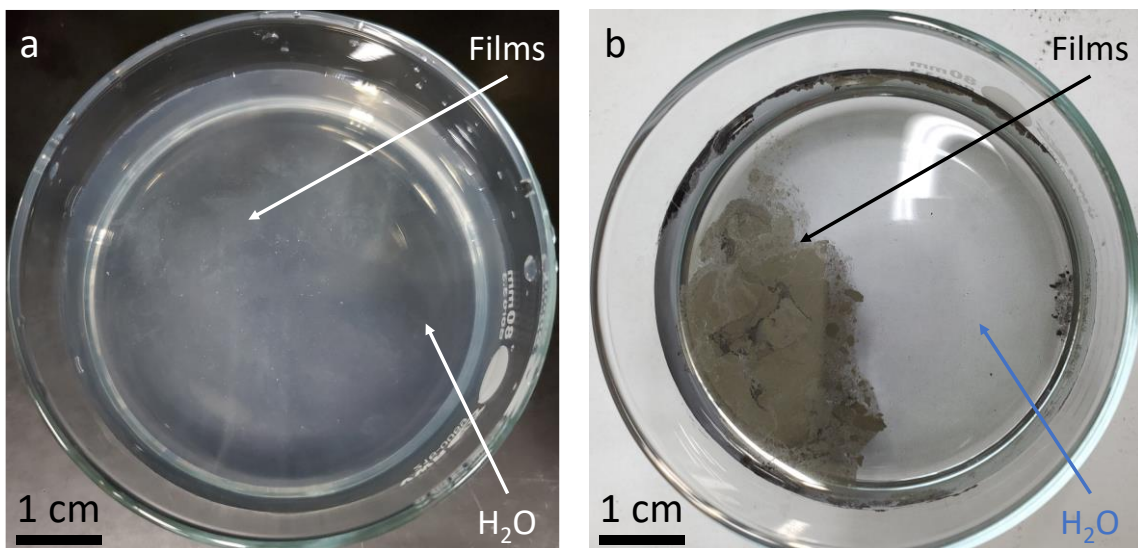


**Figure S13.** Photo of typical free standing Ni-based hydroxides films (a), and Ni-based alloy films (b).

**Preparation of nickel-based hydroxides films.** The free standing films were assembled from as-prepared nickel based hydroxides suspension by a co-solvent evaporation method.<sup>[2a]</sup> Typically, nickel-based hydroxides suspensions in ethanol (4 mL, ~5 mg/mL) was mixed with DI water (milli-Q filtered, 6 mL) and n-butanol (2.5 mL). The suspension of nickel-based hydroxides in mixed solvents was added drop by drop into a flask (about 9 cm in diameter) filled with DI water. A film of nickel-based hydroxides was then formed on the water surface and was later transferred onto the device.

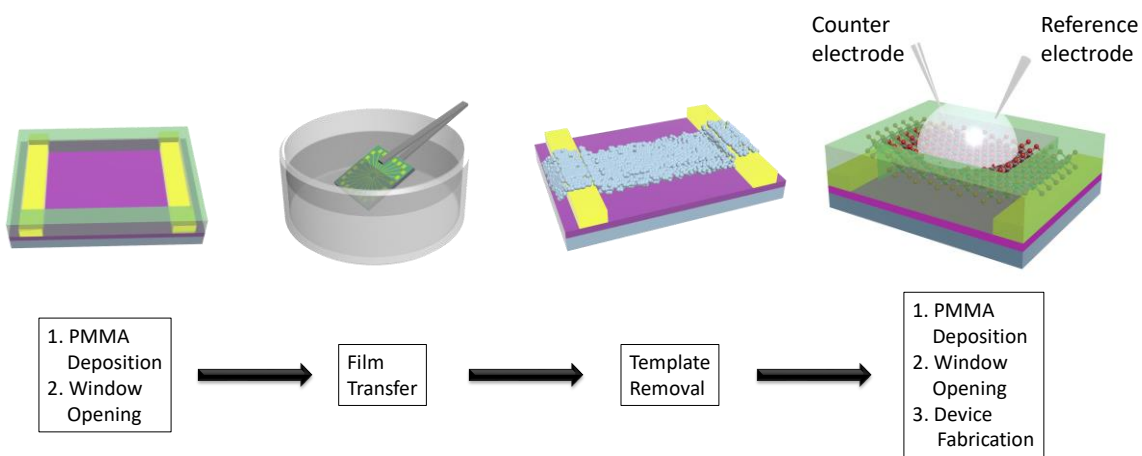


**Figure S14.** Schematic illustration of the device fabrication procedures.

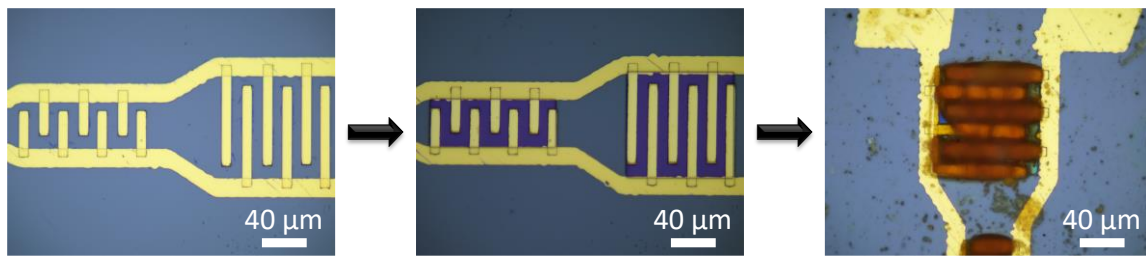


**Figure S15.** The fabrication procedures of electro-deposited NiFe hydroxides device for on-chip CV & *in situ* conductivity measurements. The electro-deposition conditions were according to the reported literatures.<sup>[10]</sup>

**Fabrication of the nickel-based hydroxides electrochemical device.**<sup>[11]</sup> Typically, a PMMA (A8, MicroChem Corp.) film was prepared by spin coating on the substrate (p+ + silicon wafer with 300 nm thermal oxide) surface with pre-patterned Ti/Au electrodes (20/50 nm). E-beam lithography was then used to open windows on PMMA, which created desired patterns on the substrate. The as-prepared (by co-solvent evaporation) free standing film of nickel-based hydroxides were then deposited onto the substrate surface. After the removal of PMMA template, nickel-based hydroxides were deposited on the device substrate with desired patterns. To eliminate the influence of electrolyte and to avoid electrochemical reactions on the metal electrodes, another layer of PMMA (electrochemically inert) was then deposited on the nickel-based hydroxides device via spin coating. A smaller window that only exposes nickel-based hydroxides was opened by e-beam lithography. In this work all of the electrochemical windows were set as 20  $\mu\text{m} \times$  30  $\mu\text{m}$  for current density normalization. The final device, with exposed nickel-based hydroxides and PMMA protected electrodes was used for on-chip electrochemistry and *in situ* electrical transport spectroscopy measurements.

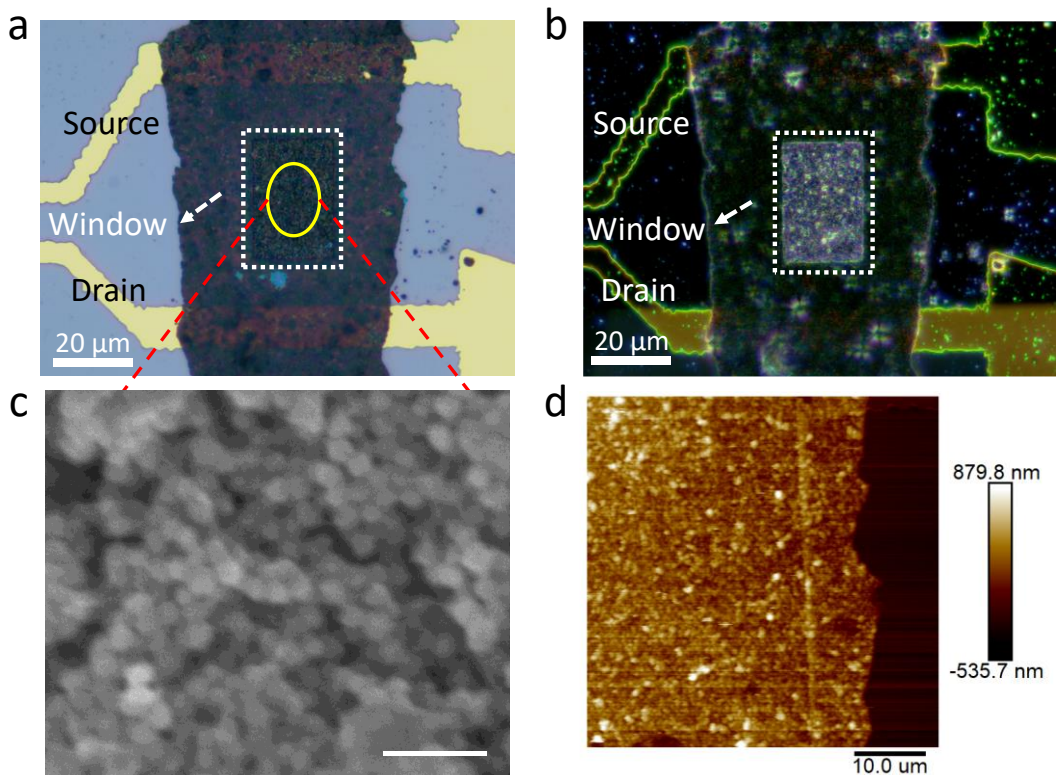


**Figure S16.** The typical optical (a), dark field optical (b), SEM (c) and AFM (d) images of the on-chip device. In this work all of the electrochemical windows were set as  $20\text{ }\mu\text{m} \times 30\text{ }\mu\text{m}$  for current density normalization. Scale bars are  $20\text{ }\mu\text{m}$ ,  $20\text{ }\mu\text{m}$ ,  $100\text{ nm}$  and  $10\text{ }\mu\text{m}$ .

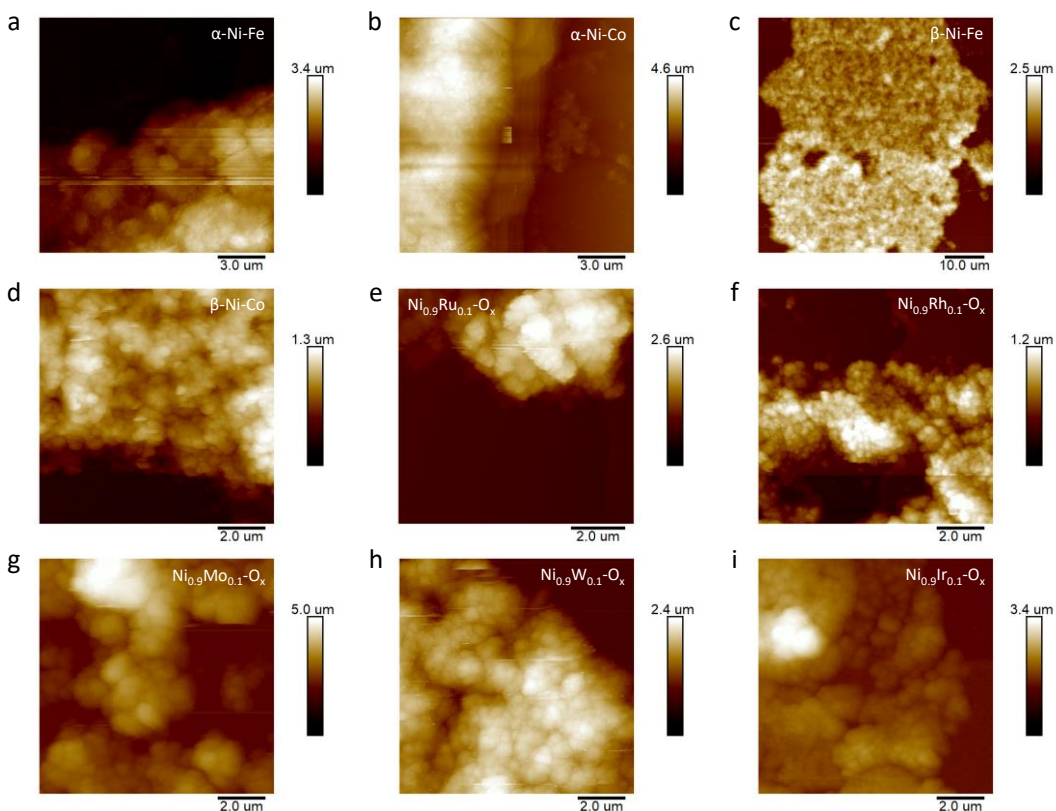


**Figure S17.** Typical AFM images of the devices (from different catalysts) tested for on-chip CV and ETS measurements, showing the general film thickness around  $1.2\sim 5.0\text{ }\mu\text{m}$ .

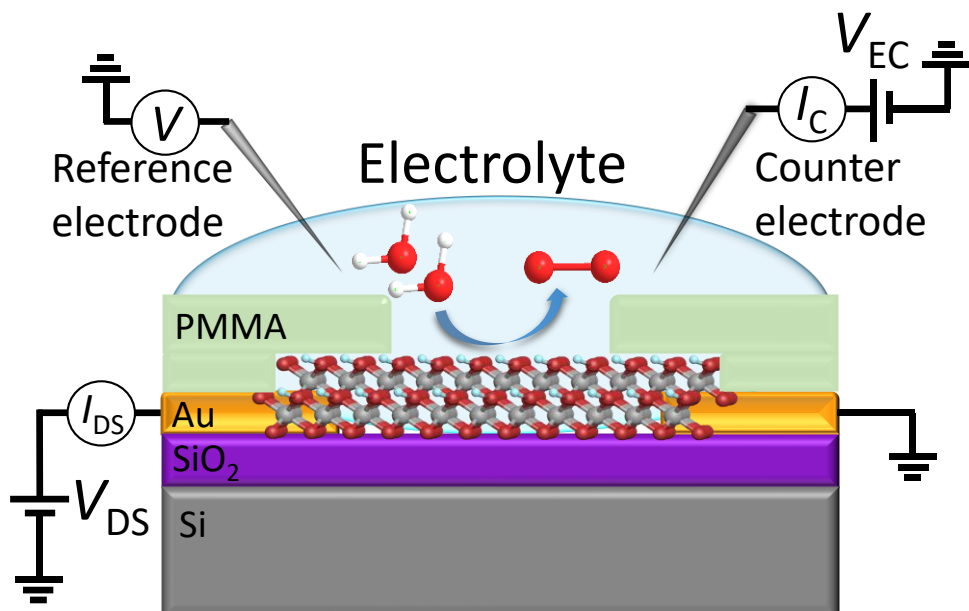


**Figure S18.** Schematic illustration of the cross-sectional view of the device.

**On-chip CV and *in situ* ETS measurements.**<sup>[11]</sup> A two channel (Source/Measure Unit) SMU (Keysight B2902a) was used for the measurement. The first SMU channel was used as a potentiostat to control the potential of source electrode as to the reference electrode ( $V_G$ ), while collecting the current ( $I_G$ ) through the counter electrode. A leak-free Ag/AgCl (Harvard Apparatus LF-2) electrode and a platinum wire were used as reference electrode and counter electrode, respectively. In a typical in-device CV measurement, the scan rate is 2 mV/s. The oxygen evolution reaction activity (OER) was evaluated in 1M KOH (99.999%, electronic grade) aqueous electrolyte. The measured potential vs.  $E_{\text{Ag/AgCl}}$  (of LF-2) was converted to reverse hydrogen electrode potential (RHE) based on the Nernst equation,  $V_{\text{RHE}} = E_{\text{vs. Ag/AgCl}} + 0.059\text{pH} + E^0$ , where  $E^0 = 0.2046$  V at 298.15 K. The electrodes were first pre-stabilized by multiple scans until reaching the steady signals to ensure hydroxides formation on the surface. The second SMU channel was used to supply a small bias voltage (50 mV) between drain and source electrodes and collecting the corresponding lateral transport current ( $I_{DS}$ ).

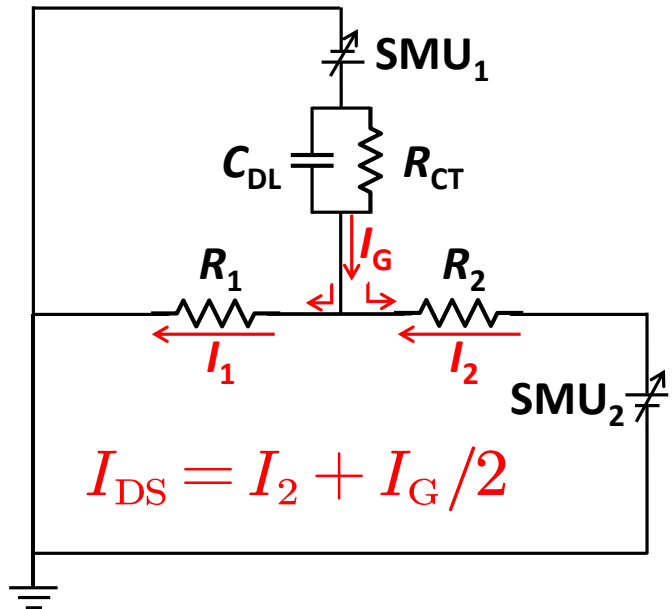


**Figure S19. Equivalent circuit model of the CV and *in situ* conductivity measurements.<sup>[11]</sup>** The contributions of  $I_G$  to  $I_{DS}$  during the measurements can be properly deducted by the equations on the bottom. For a typical measurement in this study, the Gate (Faradaic) current is smaller than the  $I_{DS}$  current. When the electrochemical current  $I_G$  is significant enough to affect the accuracy of  $I_{DS}$ , the presented equivalent circuit can be used to subtract the  $I_G$  background from the ETS ( $I_{DS}$ ) channel.

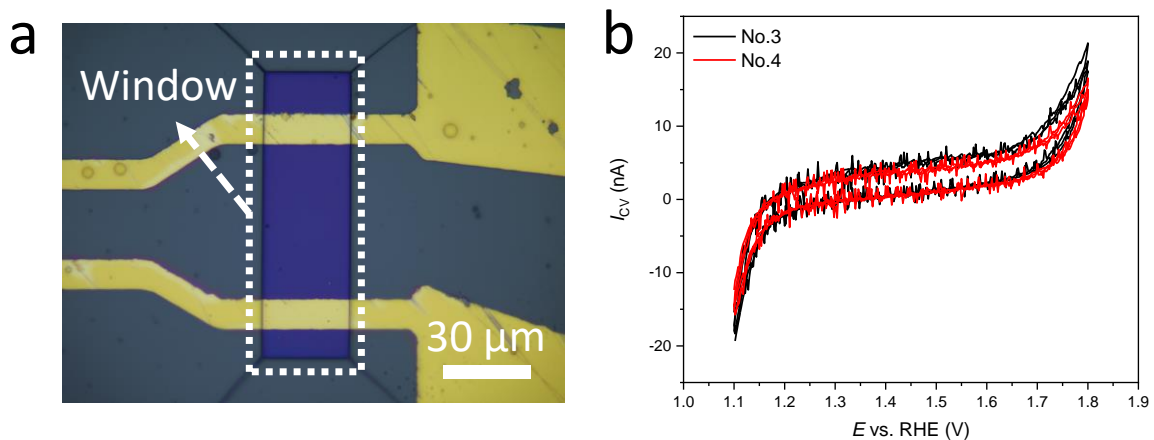


**Figure S20.** (a) The optical image of empty Au electrodes in electrochemical window (not the typical set-up for actual ETS measurements, also see Fig. S16). (b) CV curves of empty Au electrodes. Au electrodes do not show any redox features in the typical electrochemical test range of 1.15-1.7 V (vs. RHE).

## Evidences for the Hydroxides Formation after CV Activations

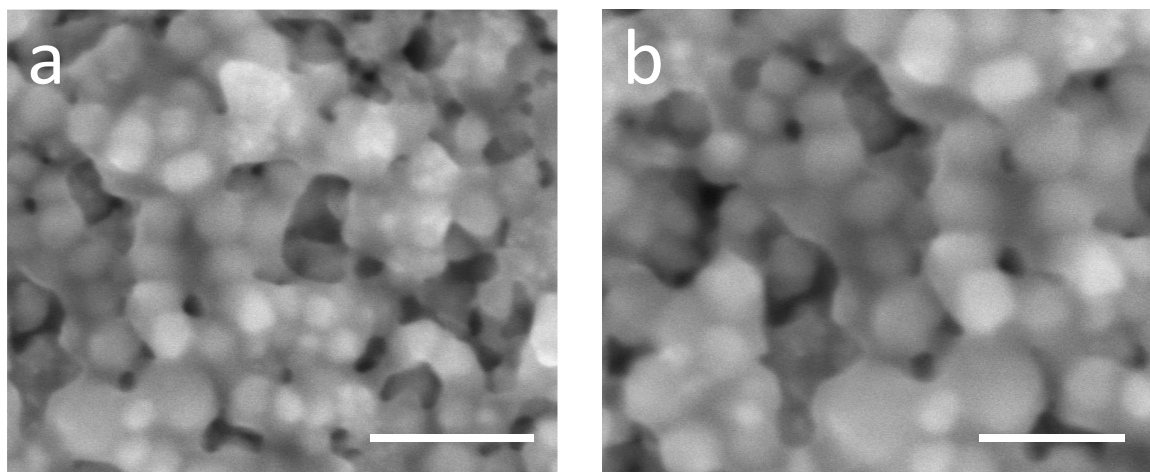


**Figure S21.** The SEM images of  $\text{Ni}_{0.9}\text{Rh}_{0.1}\text{-O}_x$  nanoparticles after CV scans, the changed morphology (compared with Fig. S4) indicated a surface reconstruction after OER.<sup>[6, 12]</sup> Scale bars are 150 nm in (a) and 100 nm in (b).

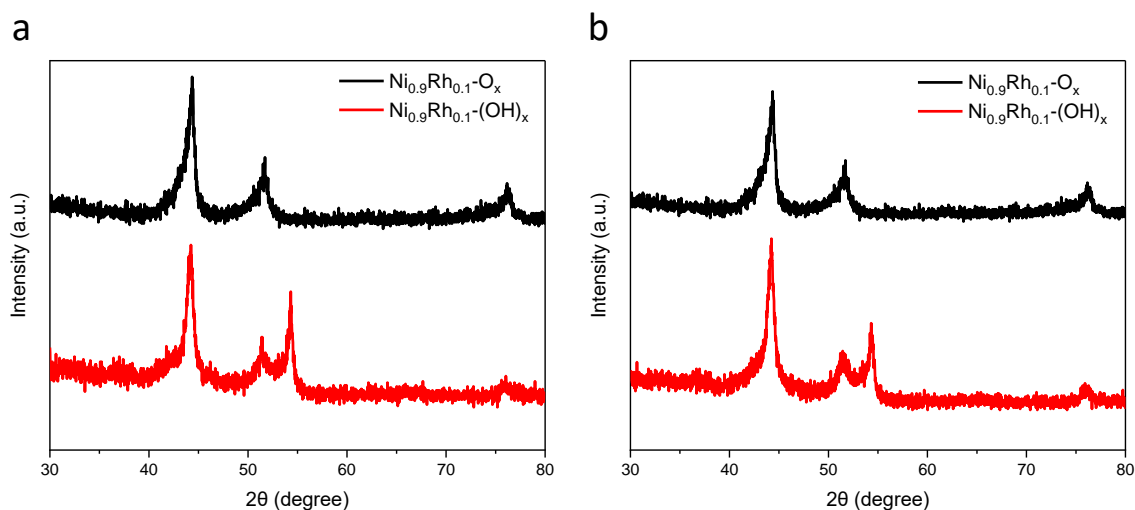


**Figure S22.** The XRD patterns of  $\text{Ni}_{0.9}\text{Rh}_{0.1}\text{-O}_x$  devices before and after CV scans. The intensity decreasing of original diffraction peaks indicate the formation of Ni-O bond and  $\text{Ni(OH)}_x$  structure.

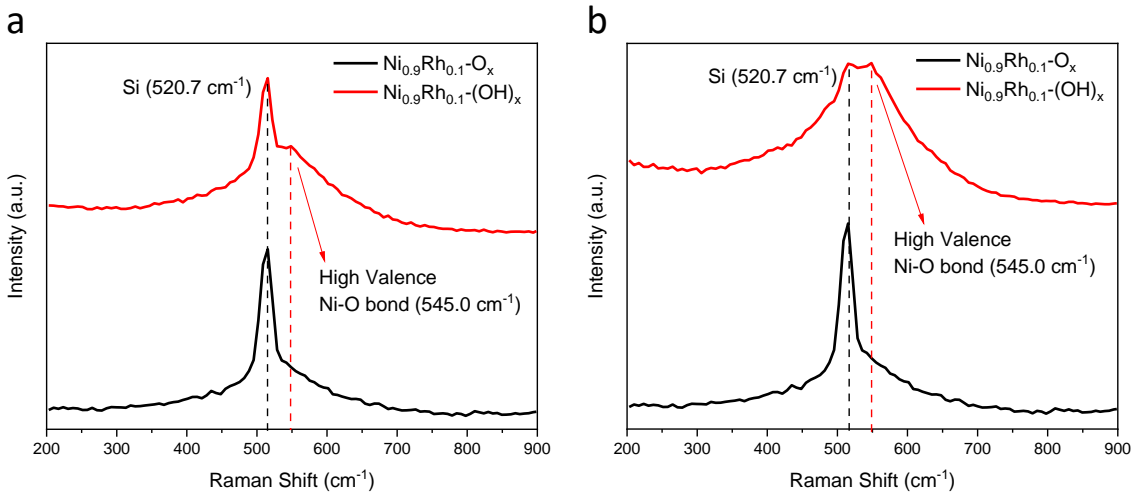


**Figure S23.** The Raman shift of  $\text{Ni}_{0.9}\text{Rh}_{0.1}\text{-O}_x$  devices before and after CV tests. The new peak ( $545.0 \text{ cm}^{-1}$ ) indicates the formation of the high-valence Ni-O bond and  $\text{Ni(OH)}_x$  structure, which is in consistence with the reported results.<sup>[12]</sup>

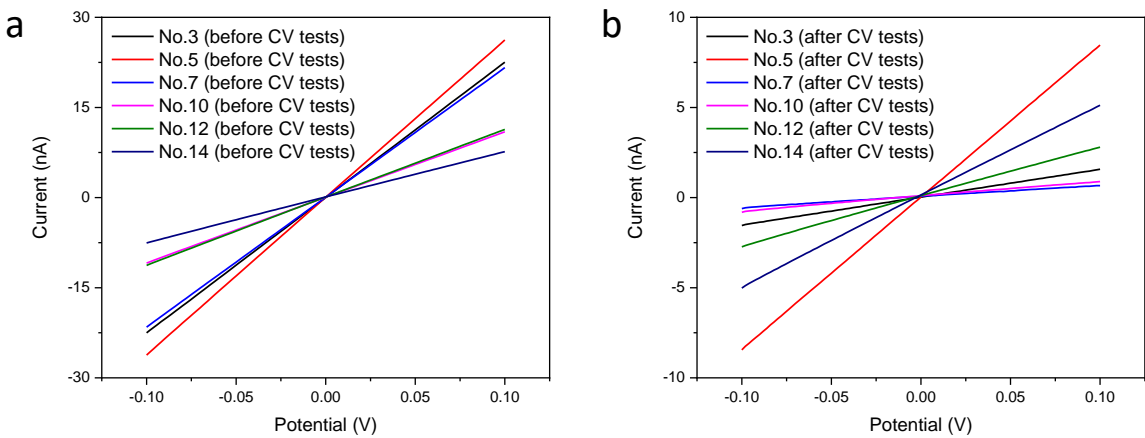


**Figure S24.** The IV tests of  $\text{Ni}_{0.9}\text{Rh}_{0.1}\text{-O}_x$  devices before CV tests (a) and after CV tests (b), it is obvious that the conductance of  $\text{Ni}_{0.9}\text{Rh}_{0.1}\text{-O}_x$  devices decreased significantly after CV scans, which indicates the hydroxides formation after CV scans. The I-V tests were conducted in the vacuum probe station (Lake Shore CRYOTRONICS) at pressure  $< 5 \times 10^{-4}$  Torr.

For the  $\text{Ni}_{0.9}\text{Mo}_{0.1}\text{-O}_x$ ,  $\text{Ni}_{0.9}\text{W}_{0.1}\text{-O}_x$ ,  $\text{Ni}_{0.9}\text{Ru}_{0.1}\text{-O}_x$  and  $\text{Ni}_{0.9}\text{Rh}_{0.1}\text{-O}_x$  devices, after the CV scans the initial conductivities (near zero) were small enough to prove the formation of corresponding hydroxides. Only the strong double exchange interaction in the lattice of the OER active intermediates can account for the high *in situ* conductance, and the approximate  $0.1\text{-}0.6 \mu\text{A } I_{\text{DS}}$  currents further confirm the *in situ* conductivity originated from  $\gamma\text{-Ni}_{0.9}\text{Ru}_{0.1}\text{OOH}$  and  $\gamma\text{-Ni}_{0.9}\text{Rh}_{0.1}\text{OOH}$  for  $\text{Ni}_{0.9}\text{Ru}_{0.1}\text{-O}_x$  and  $\text{Ni}_{0.9}\text{Rh}_{0.1}\text{-O}_x$  devices. However, the *in situ* conductivity of  $\text{Ni}_{0.9}\text{Mo}_{0.1}\text{-O}_x$  and  $\text{Ni}_{0.9}\text{W}_{0.1}\text{-O}_x$  were relatively low, which indicates the double exchange interaction doesn't exist in their OER active intermediates.

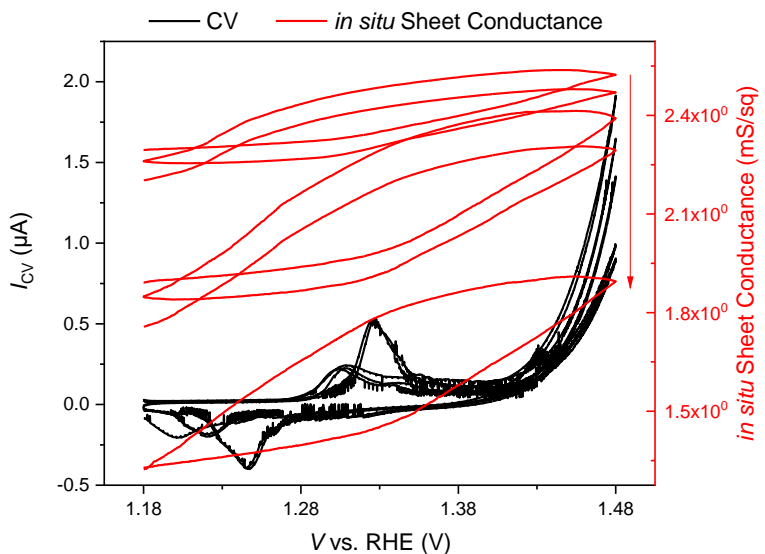


**Figure S25.** The slow (2 mV/s) CV scans of  $\text{Ni}_{0.9}\text{Ir}_{0.1}\text{-O}_x$  devices before CV & ETS tests. The continuously dropped *in situ* Sheet Conductance and changed shape of CV curves indicate the hydroxides formation after CV scans.

Due to the violent bubble overflow during OER will cause great damage to the devices, the number of slow (2 mV/s) CV scans was kept as 5-7 cycles to make sure the device in a stabilized state (the values of initial and ending sheet conductance were almost the same). If the  $\text{Ni}_{0.9}\text{Ir}_{0.1}\text{-O}_x$  species always kept as alloy during OER, the *in situ* sheet conductance won't be further increased compared with the current of initial phase. Therefore, the further improved large *in situ* conductance confirmed the conductivity originated from OER active intermediates ( $\gamma\text{-Ni}_{0.9}\text{Ir}_{0.1}\text{OOH}$ ).

## Exclude the Influence of Oxygen Vacancies and Morphology

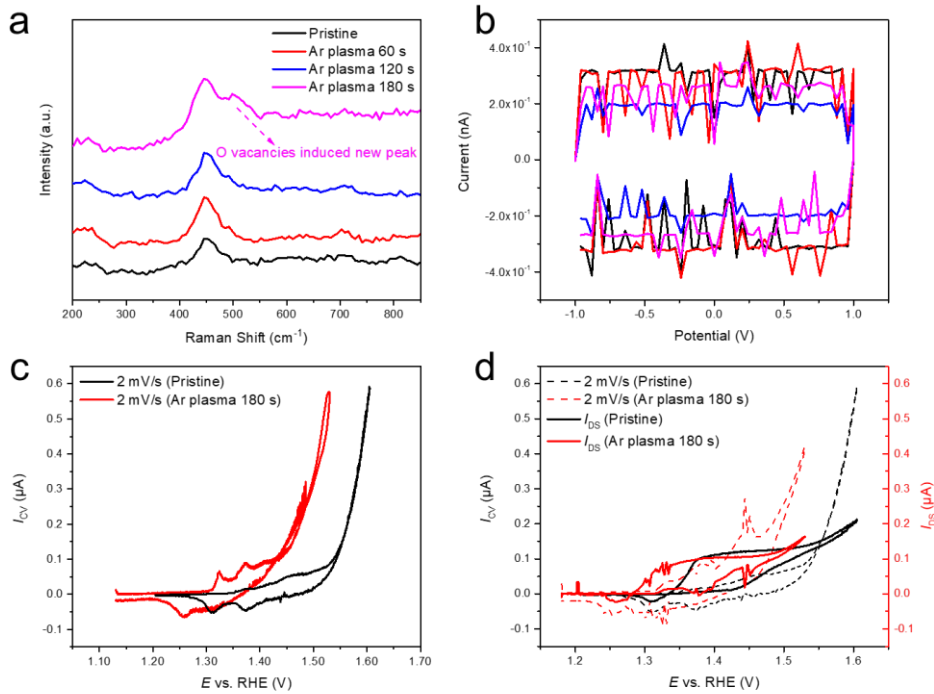


**Figure S26.** The characterization, on-chip OER and *in situ* transport measurement of  $\alpha\text{-Ni(OH)}_2$  samples with different amount of oxygen vacancies (treated by Ar plasma with different times, 13.56 MHz RF source, 250 W and 200 SCCM<sup>[13]</sup>). (a) Raman spectra indicated the successful introduction of O vacancies. (b) The I-V test of the same device with different amount of O vacancies showed almost no change in baseline conductivity. (c,d) The on-chip CV (c) and *in situ* conductance measurements (d) demonstrated the improved OER performance with more O vacancies, which showed negligible influence on the *in situ* intermediate conductivities.

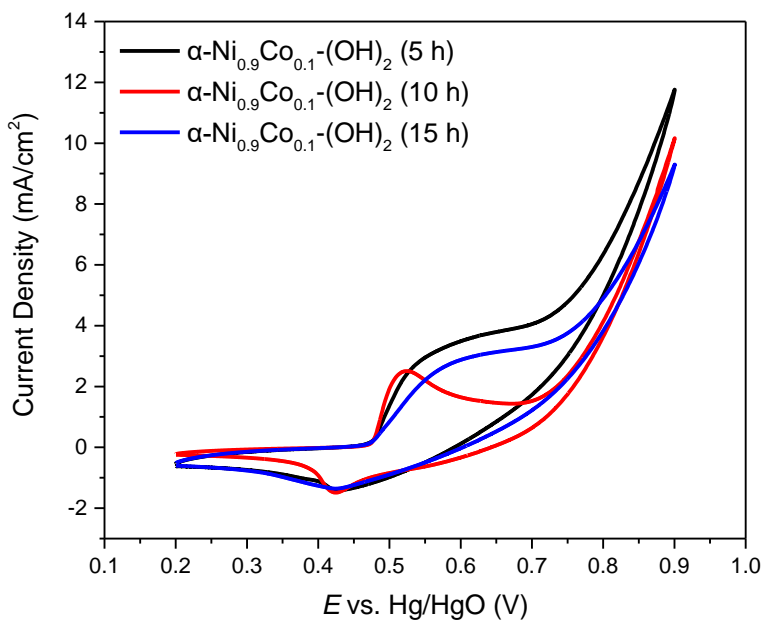


**Figure S27.** The CV curves of  $\alpha\text{-Ni}_{0.9}\text{Co}_{0.1}\text{-(OH)}_2$  catalysts with controlled size through different reaction time (5 h  $\sim$   $< 1 \mu\text{m}$ , 10 h  $\sim 2 \mu\text{m}$ , 15 h  $\sim 3\text{-}4 \mu\text{m}$ , morphology shown in Fig. S6), the catalytic activity showed low dependence on particle size.

## Bulk OER Electrochemical Test of the Catalysts

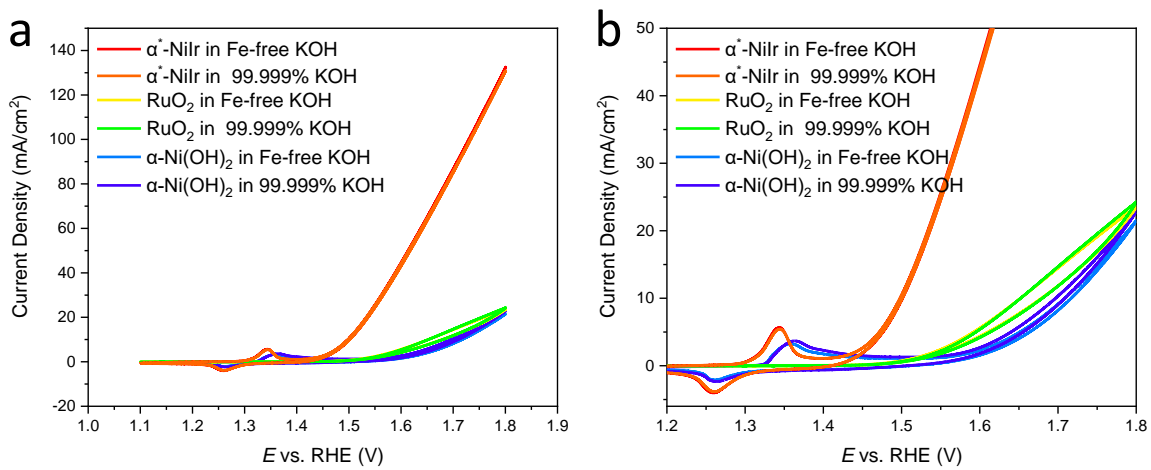


**Figure S28.** The comparison of bulk electrochemical catalytic activity of  $\alpha^*\text{-NiIr}$ , commercial  $\text{RuO}_2$  and  $\alpha\text{-Ni(OH)}_2$  in 1 M KOH (99.999%) and Fe-free 1 M KOH electrolyte. Figure b is an enlarged Figure a. The scan rate is 5 mV/s.

## Separated CV & ETS results of Electrocatalysts with DE Interaction

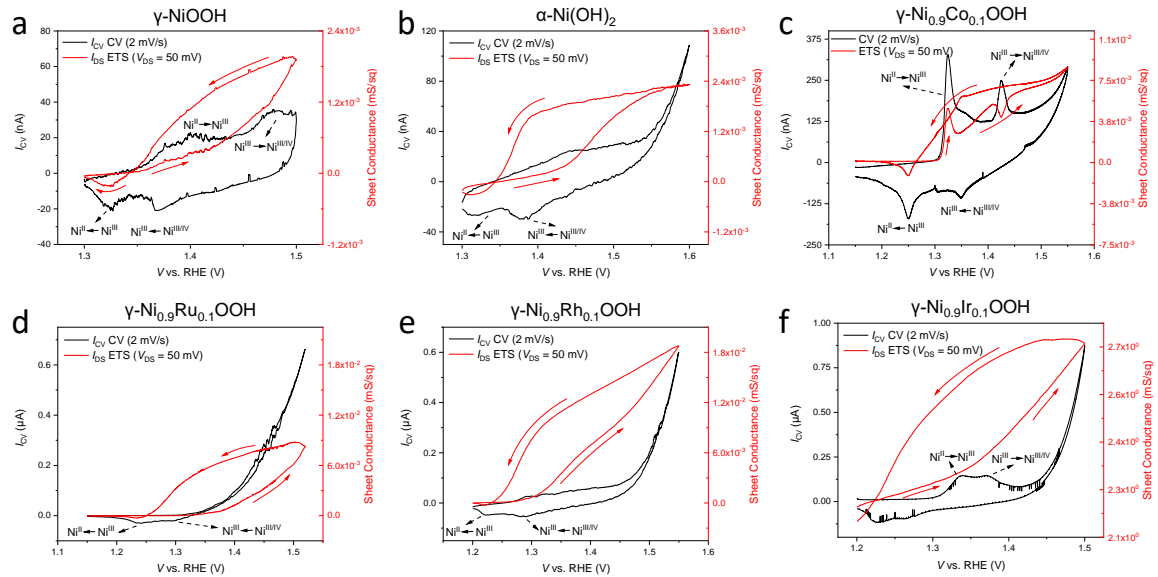


**Figure S29.** The separated CV & ETS results of electrocatalysts with double exchange interaction (relatively higher *in situ* conductance). The potential of conductivity sharp increase and Ni<sup>III/IV</sup> oxidation potential exactly match with each other, and the conductivity decrease to the initial state with the complete reduction of Ni<sup>III/IV</sup>.

According to the results in Figure S28, as the electrochemical potential is changed, the appearance and disappearance of Ni<sup>III/IV</sup> has the largest effect on the change in conductivity of the catalyst. During the electrochemical reaction, electrons are transported through the semiconductor/conductor electrocatalyst, accompanied by the *in situ* conductivity (ETS) curves, thus we can consider that the intermediate with higher conductivity in a particular catalytic system has higher catalytic activity.<sup>[14]</sup> That is, the high-valence Ni<sup>III/IV</sup> is the catalytic active species towards OER.

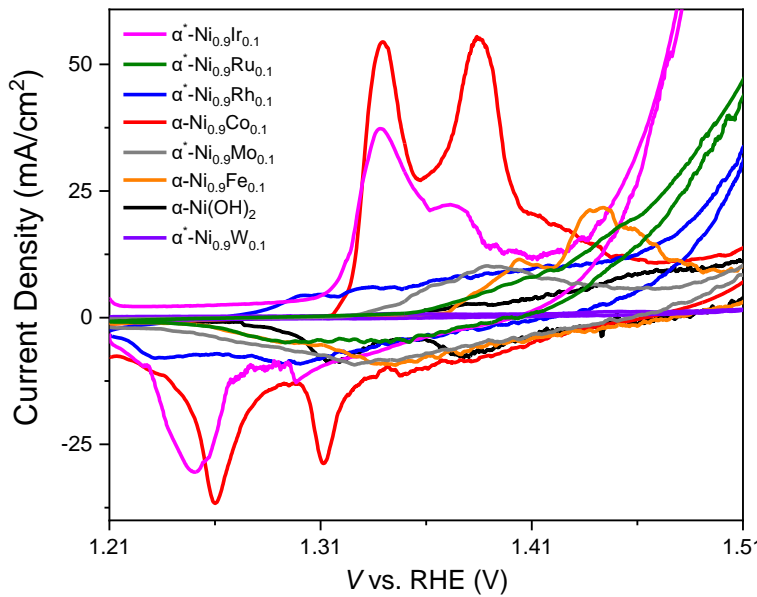


**Figure S30.** The zoomed figure prior to OER for clearly observing the redox peaks of each catalyst.

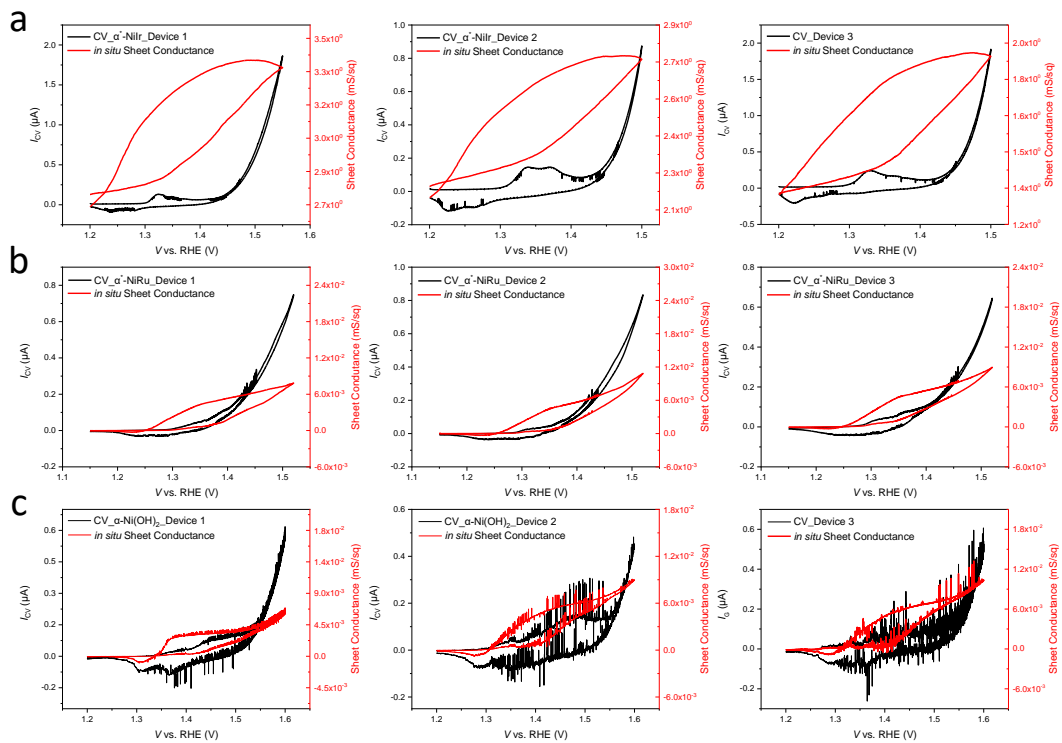


**Figure S31.** On-chip CV and *in situ* conductance (ETS) results from three different devices for  $\alpha^*\text{-Ni}_{0.9}\text{-Ir}_{0.1}(\text{OH})_2$  (a),  $\alpha^*\text{-Ni}_{0.9}\text{-Ru}_{0.1}(\text{OH})_2$  (b) and  $\alpha\text{-Ni}(\text{OH})_2$  (c). The CV and ETS characteristic (insulator-semiconductor phase transition) can be well reproduced (scan rate is 2 mV/s).

**Table S1.** The detailed electrochemical potential information for each electrocatalyst, the catalysts with higher *in situ* conductance were marked out with rose red color.

Catalysts vs. RHE	Conductivity onset (V)	Second oxidation peak onset (V)	OER onset (V)	OER potential (V) @10 mA/cm <sup>2</sup>	<i>in situ</i> Sheet Conductance (mS/sq)
$\alpha^*$ -Ni <sub>0.9</sub> -Ir <sub>0.1</sub>	1.35	1.36	1.42	1.43	1.89×10 <sup>0</sup>
$\alpha^*$ -Ni <sub>0.9</sub> -Ru <sub>0.1</sub>	1.42	1.42	1.45	1.46	6.58×10 <sup>-3</sup>
$\alpha^*$ -Ni <sub>0.9</sub> -Rh <sub>0.1</sub>	1.31	1.37	1.47	1.48	1.55×10 <sup>-2</sup>
$\alpha^\triangle$ -Ni <sub>0.9</sub> -Fe <sub>0.1</sub>	1.40	--	1.45	1.48	1.89×10 <sup>-3</sup>
$\alpha$ -Ni <sub>0.9</sub> -Co <sub>0.1</sub>	1.38	1.41	1.50	1.51	9.12×10 <sup>-3</sup>
$\alpha$ -Ni <sub>0.9</sub> -Fe <sub>0.1</sub>	1.40	1.41	1.51	1.52	4.98×10 <sup>-4</sup>
$\alpha$ -Ni(OH) <sub>2</sub>	1.44	1.45	1.52	1.53	4.09×10 <sup>-3</sup>
$\alpha^*$ -Ni <sub>0.9</sub> -Mo <sub>0.1</sub>	1.35	1.37	1.49	1.50	5.25×10 <sup>-4</sup>
$\alpha^*$ -Ni <sub>0.9</sub> -W <sub>0.1</sub>	1.41	1.42	1.51	1.60	7.29×10 <sup>-4</sup>
$\beta$ -Ni <sub>0.9</sub> -Fe <sub>0.1</sub>	1.40	1.41	1.46	1.51	8.25×10 <sup>-4</sup>
$\beta$ -Ni <sub>0.9</sub> -Co <sub>0.1</sub>	1.40	1.40	1.49	1.52	7.86×10 <sup>-4</sup>
$\beta$ -Ni(OH) <sub>2</sub>	1.43	1.45	1.54	1.60	4.89×10 <sup>-4</sup>

## Comparisons of $iR$ & $\Delta\eta$ at Sequential Integral Current Densities

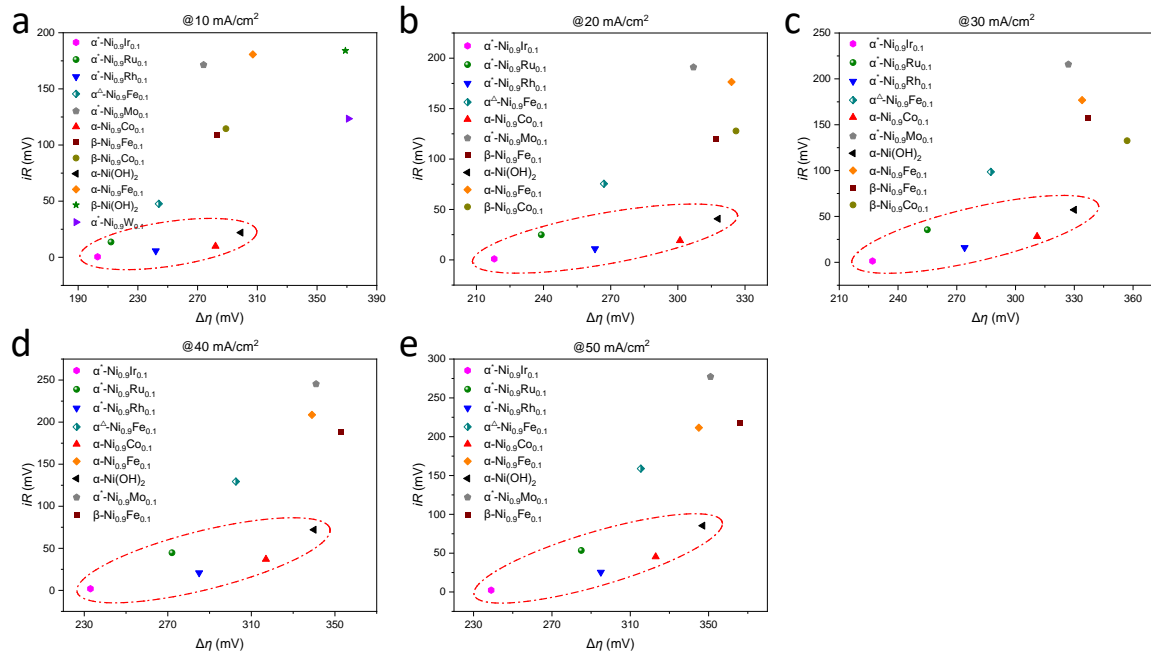


**Figure S32.** The comparisons of overpotential  $\Delta\eta$  and  $iR$  derived from the *in situ* conductance @10 mA/cm<sup>2</sup> (a), (b) @20 mA/cm<sup>2</sup>, (c) @30 mA/cm<sup>2</sup>, (d) @40 mA/cm<sup>2</sup>, and (e) @50 mA/cm<sup>2</sup>. It is evident that the potential drop caused by the internal resistance ( $iR$ ) accounts for only a small part of the overpotential ( $\Delta\eta$ ), especially for the catalysts with increased DE interactions (higher *in situ* conductance), as indicated by dashed cycles in (a), (b), (c), (d) and (e). “ $\alpha^*$ ” denotes pre-oxidation with CV cycles to achieve  $\alpha$ -hydroxide formation on the surface. “ $\alpha^\Delta$ ” denotes Fe<sup>III</sup> ion exchange treated pure  $\alpha$ -Ni(OH)<sub>2</sub>.

After analysis, we can conclude that catalysts (Co, Rh, Ir doped  $\gamma$ -NiOOH) showing synergistic catalytic effects and strong exchange interaction (higher *in situ* conductance) demonstrate relatively lower overpotential and smaller Tafel slope. Catalysts (such as Ru doped  $\gamma$ -NiOOH) with only moderate exchange interaction can lead to a relatively lower overpotential but slow kinetics, while catalysts (Mo, W doped  $\gamma$ -NiOOH and  $\beta$ -NiOOH) without synergistic catalytic effect or any exchange interaction (low *in situ* conductance) are usually not good candidates for OER because of the too large internal resistance.

## Systematic Mechanism Investigation of other NiFe Hydroxides

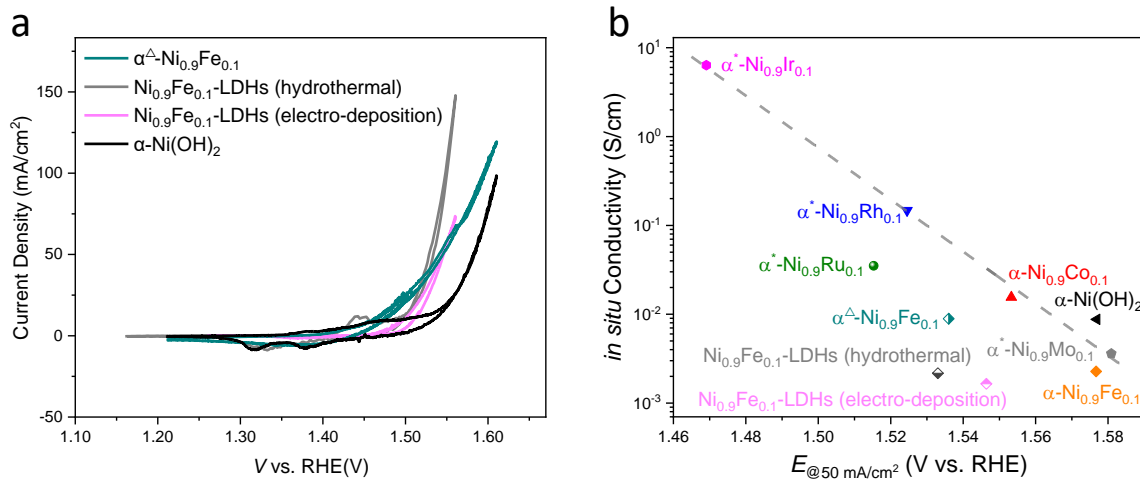


**Figure S33.** (a) The on-chip OER performance of NiFe-LDHs (through hydrothermal preparation and NiFe electro-deposition), and  $\alpha$ -NiFe through Fe<sup>III</sup> ion-exchange. (b) Summary of *in situ* conductivity and OER activity (quantified by the overpotential @50 mA/cm<sup>2</sup>) of  $\alpha$  phase  $\text{Ni}_{0.9}\text{M}_{0.1}\text{-OOH}$ . “ $\alpha^*$ ” denotes pre-oxidation with CV cycles to achieve  $\alpha$ -hydroxide formation on the surface. “ $\alpha^{\Delta}$ ” denotes the doped  $\alpha$ -hydroxide prepared via Fe<sup>III</sup> ion exchange approach.

These different activity-conductivity correlations are interesting and can indicate different OER mechanisms in these compositionally similar NiFe samples (another indication is that different Tafel slopes observed in these samples). For the ion-exchange sample, because the ion exchange process was induced after the same preparation approach of  $\alpha\text{-Ni(OH)}_2$ , this sample can be considered as most similar to the original system, and therefore matches best to the original trend. When hydrothermal and electro-deposition methods were employed, layered double hydroxide (LDH) structures were formed (as reported in corresponding literatures, and can also be indicated from our XRD results). The mechanisms of  $\text{Ni}_{0.9}\text{Fe}_{0.1}$  LDHs are generally believed to be different with other metal doped Ni hydroxides.<sup>[15]</sup> In Ni-Fe LDHs, the OER active site is Fe rather than Ni, and the oxidation state of Fe remained at +3 during OER (ref<sup>[16]</sup> reported that Fe remained at +3 state during OER), while neither Ni<sup>III/IV</sup> nor the oxygen radical character on Fe<sup>IV</sup> (state 4) existed in OER. Since the DE interaction occurred in the system that M-O bonds have high covalency (high oxidation states), low *in situ* conductivity was observed in  $\text{Ni}_{0.9}\text{Fe}_{0.1}$  hydrothermal LDHs and electro-deposited Ni-Fe LDHs. **In conclusion, Fe doping in the  $\alpha\text{-Ni(OH)}_2$  can result in complicated consequences in terms of crystallinity, OER activity and mechanism. With proper synthetic approach,  $\alpha^{\Delta}\text{-Ni}_{0.9}\text{Fe}_{0.1}\text{(OH)}_2$  (through ion-exchange in this study) showed expected improved OER activity and matching trend in activity-conductivity correlation. In all different cases, *in situ* conductivity was fundamentally determined by the high oxidation states on Ni<sup>III/IV</sup> site (and consequently the higher degree of DE interaction), and its different characteristics can effectively reveal the different OER mechanisms.** Additionally, it can be more clearly noted in the Figure 4a that  $\alpha^*\text{-Ni}_{0.9}\text{Ru}_{0.1}\text{(OH)}_2$  and  $\alpha^{\Delta}\text{-Ni}_{0.9}\text{Fe}_{0.1}\text{(OH)}_2$  show a slight shift to the linear correlation in Ir, Rh, Co, and pristine cases, which matched to the previous prediction that promotion of radical characters in metal-oxo bond mechanism exist in Ir, Rh, Co cases but not in Ru, Mo, and W cases. In Fe case, the mechanism is complicated, which may involve the combination/competition between two mechanistic pathways.

### Stability Test of $\alpha^*$ -Ni<sub>0.9</sub>Ir<sub>0.1</sub> Catalyst

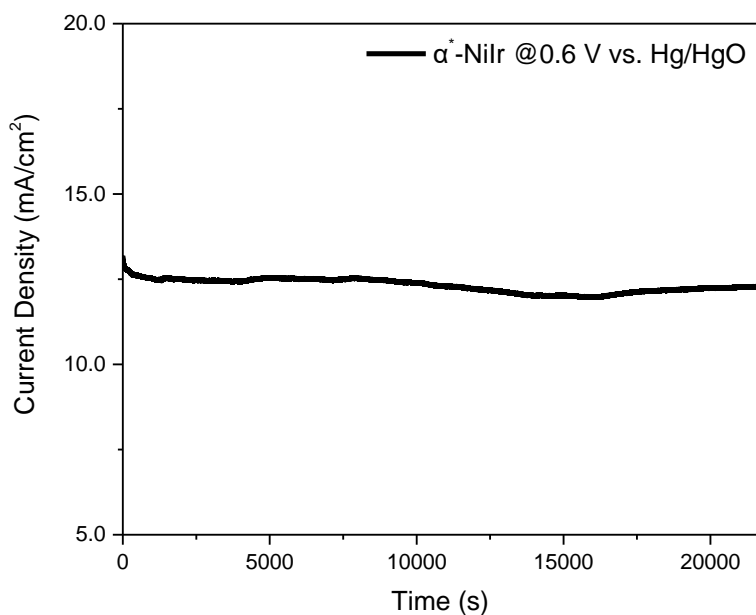


**Figure S34.** The stability test of the  $\alpha^*$ -Ni<sub>0.9</sub>Ir<sub>0.1</sub> catalyst at large current density.

## Post-OER XRD Patterns and XPS Spectra

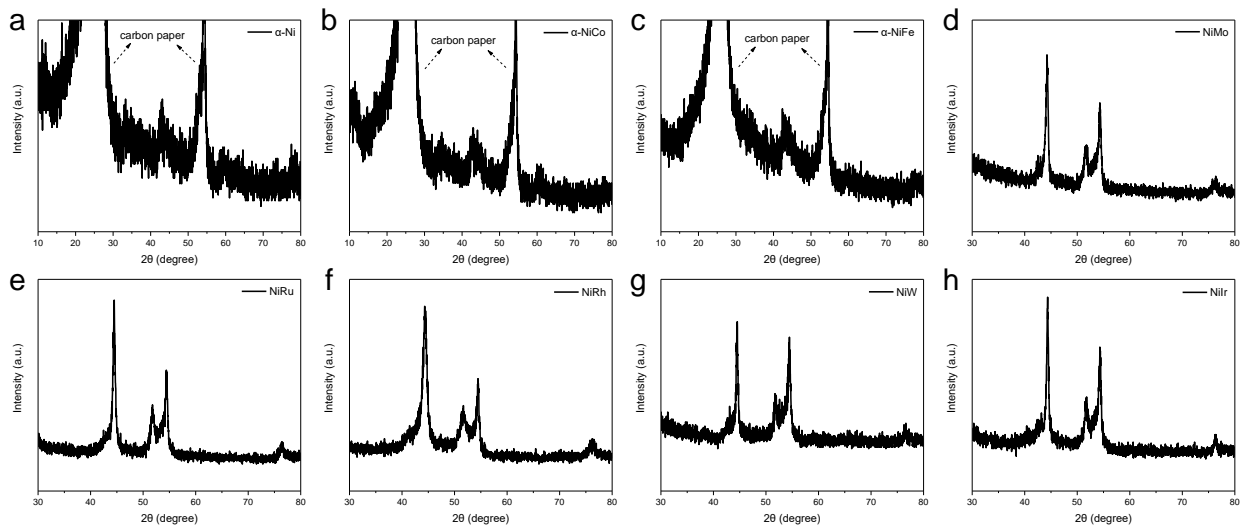


**Figure S35.** The post-OER (electrolysis at 0.8 V vs. Hg/HgO for 3hr) XRD patterns of different metal doped NiOOH catalysts. The decreased intensity of 2θ peaks indicated the formation of more amorphous oxyhydroxide on the surface.

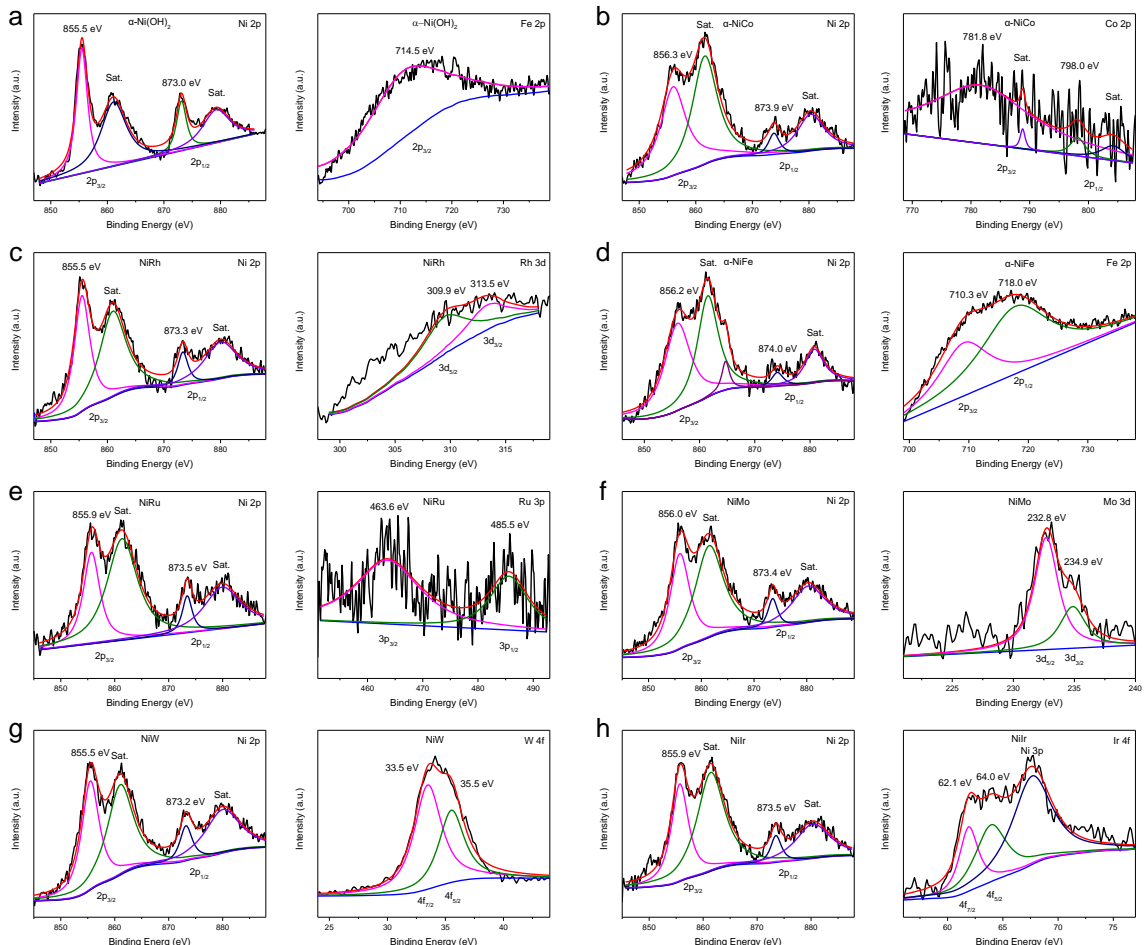


**Figure S36.** The post-OER (electrolysis at 0.8 V vs. Hg/HgO for 3hr) XPS spectra of a series of metal doped NiOOH. (a) The Ni and Fe 2p peaks in  $\alpha$ -Ni(OH)<sub>2</sub>. (b) The Ni and Co 2p peaks in  $\alpha$ -NiCo-(OH)<sub>2</sub>. (c) The Ni 2p peaks and Rh 3d peaks in  $\alpha^*$ -NiRh. (d) The Ni 2p peaks and Fe 2p peaks in  $\alpha$ -NiFe-(OH)<sub>2</sub>. (e) The Ni 2p peaks and Ru 3d peaks in  $\alpha^*$ -NiRu. (f) The Ni 2p peaks

and Mo 3d peaks in  $\alpha^*$ -NiMo. (g) The Ni 2p peaks and W 4f peaks in  $\alpha^*$ -NiW. (h) The Ni 2p peaks and Ir 4f peaks in  $\alpha^*$ -Nilr. The increased binding energy of characteristic peaks of Ni and doped metal indicated the formation of oxidized oxyhydroxide on the surface. Black curves depict the original XPS spectra and colored curves represent the fitted peaks.

The binding energy of Ni 2p peaks in post-OER  $\alpha$ -Ni(OH)<sub>2</sub> indicated the valence state was around  $\geq +3$  for Ni. The binding energy of Ni 2p and Co 2p peaks in post-OER  $\alpha$ -Ni<sub>0.9</sub>Co<sub>0.1</sub>(OH)<sub>2</sub> indicated the valence states of Ni and Co were around  $\geq +3$  and  $\geq +3$ , respectively. The binding energy of Ni 2p and Rh 3d peaks in post-OER  $\alpha^*$ -Ni<sub>0.9</sub>Rh<sub>0.1</sub> indicated the valence states of Ni and Rh were around  $\geq +3$  and  $\geq +3$ , respectively. The binding energy of Ni 2p and Fe 2p peaks in post-OER  $\alpha$ -Ni<sub>0.9</sub>Fe<sub>0.1</sub>(OH)<sub>2</sub> indicated the valence states of Ni and Fe were around  $\geq +3$  and  $+2 \sim +3$ , respectively. The binding energy of Ni 2p and Ru 3p peaks in post-OER  $\alpha^*$ -Ni<sub>0.9</sub>Ru<sub>0.1</sub> indicated the valence states of Ni and Ru were around  $\geq +3$  and  $\geq +3$ , respectively. The binding energy of Ni 2p and Mo 3d peaks in post-OER  $\alpha^*$ -Ni<sub>0.9</sub>Mo<sub>0.1</sub> indicated the valence states of Ni and Mo were around  $+3$  and  $+5$ , respectively. The binding energy of Ni 2p and W 4f peaks in post-OER  $\alpha^*$ -Ni<sub>0.9</sub>W<sub>0.1</sub> indicated the valence states of Ni and W were around  $+3$  and  $+5$ , respectively. The binding energy of Ni 2p and Ir 4f peaks in post-OER  $\alpha^*$ -Ni<sub>0.9</sub>Ir<sub>0.1</sub> indicated the valence states of Ni and Ir were around  $\geq +3$  and  $+3 \sim +4$ , respectively. The attribution of all the peaks is based on the standard database (<https://srdata.nist.gov/xps/Default.aspx>).

## Illustration of Possible DE interactions for $\alpha^*\text{-Ni}_{0.9}\text{Ru}_{0.1}$ Catalyst

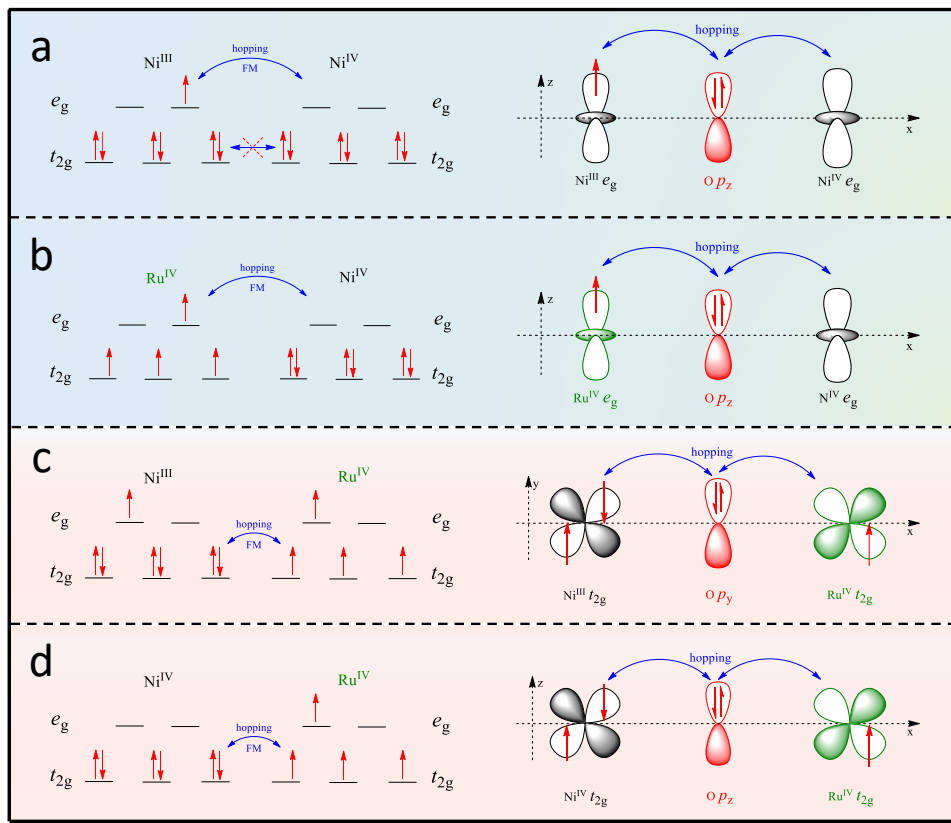


**Figure S37.** Schematic illustration of how the double exchange (DE) interaction can provide conductive pathways in the lattice of  $\gamma\text{-Ni}_{0.9}\text{Ru}_{0.1}\text{OOH}$ . The schematic illustration of DE interaction of  $e_g$  orbitals between  $\text{Ni}^{\text{III}}$  and  $\text{Ni}^{\text{IV}}$  (a),  $\text{Ni}^{\text{III}}$  and  $\text{Ru}^{\text{IV}}$  (b). Illustration of DE interaction of  $t_{2g}$  orbitals between  $\text{Ni}^{\text{III}}$  and  $\text{Ru}^{\text{IV}}$  (c),  $\text{Ni}^{\text{IV}}$  and  $\text{Ru}^{\text{IV}}$  (d). And super-exchange (SE) interaction of  $t_{2g}$  orbitals between  $\text{Ru}^{\text{IV}}$  ions was omitted. The DE interactions of  $t_{2g}$  orbitals between Ni and Ru may not be weaker due to the energy level mismatch<sup>[17]</sup> and hence weaker DE interaction compared with Co/Rh/Ir doped  $\gamma\text{-NiOOH}$ . The left part in all of the figures is the d orbital occupancy of two adjacent metal ions, the right part is the DE interaction, and the spatial orientation of d orbitals is also taken into consideration. FM, ferromagnetic; AFM, antiferromagnetic.

### Illustration of Catalysts cannot undergo DE interactions

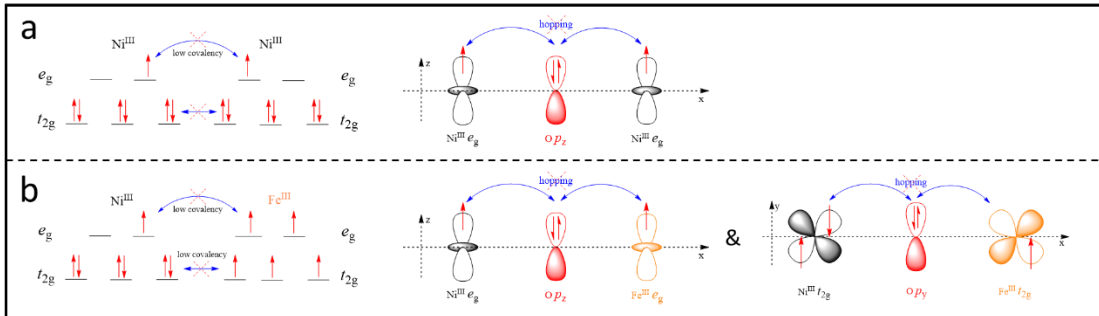


**Figure S38.** Schematic illustration of inefficient double exchange (DE) interaction in the lattice of  $\text{Ni}_{0.9}\text{Fe}_{0.1}$ -LDHs. Due to different OER mechanisms of  $\text{Ni}_{0.9}\text{Fe}_{0.1}$ -LDHs<sup>[15-16]</sup> and low covalencies of  $\text{Ni}^{\text{III}}\text{-O-Fe}^{\text{III}}$  bonds, the electrons cannot hop through the bridged oxygen  $p$  orbitals between  $\text{Ni}^{\text{III}}\text{-Fe}^{\text{III}}$  sites.

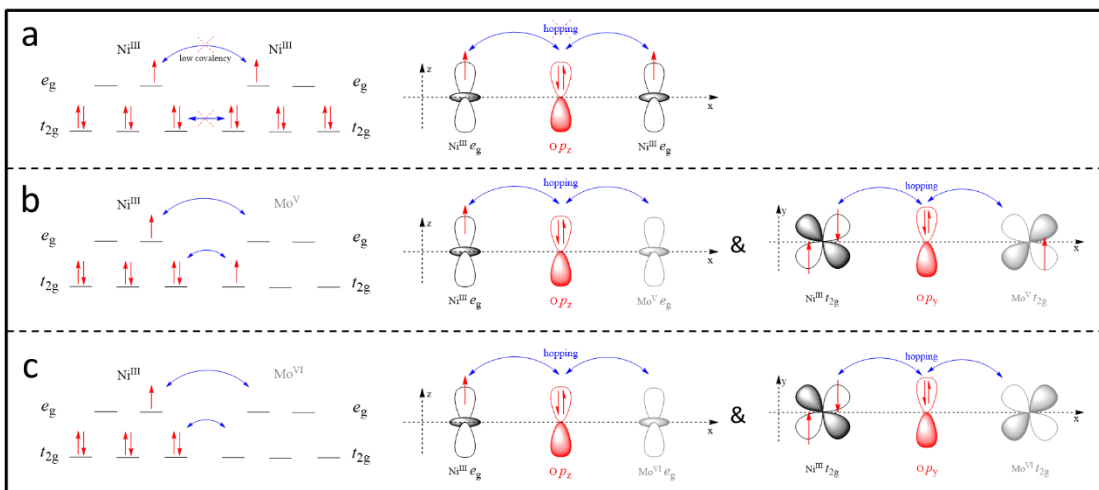


**Figure S39.** Schematic illustration of the possible double exchange (DE) interaction in the lattice of  $\text{Ni}_{0.9}\text{Mo}_{0.1}\text{-O}_x$ . It was reported that the incorporation of high valence metal (Mo, W) would change the oxidation behavior of Ni and Fe (remain low oxidation state during OER),<sup>[18]</sup> and thus the weak electrons hopping which cannot provide effective conductive pathways.

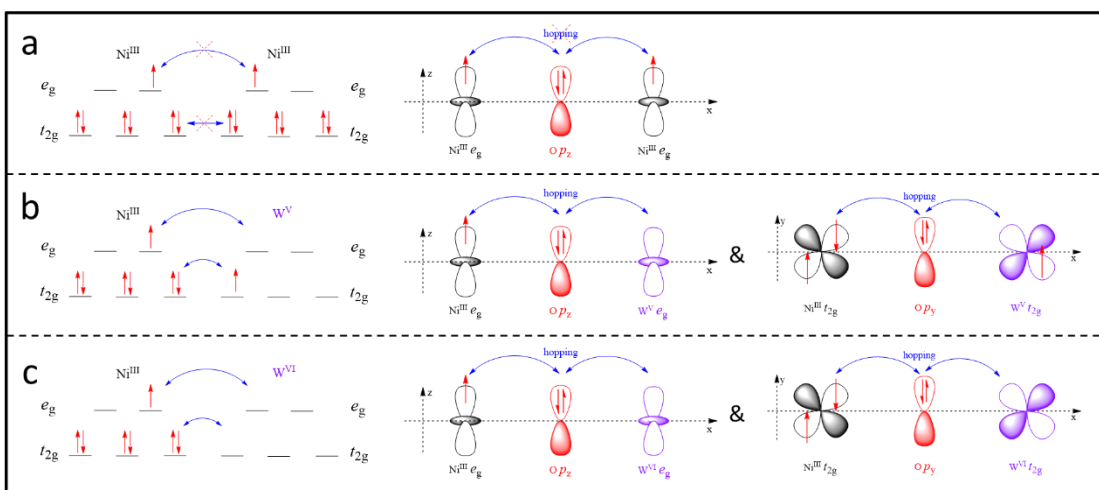


**Figure S40.** Schematic illustration of the possible double exchange (DE) interaction in the lattice of  $\text{Ni}_{0.9}\text{W}_{0.1}\text{-O}_x$ . It was reported that the incorporation of high valence metal (Mo, W) would change the oxidation behavior of Ni and Fe (remain low oxidation state during OER),<sup>[18]</sup> and

thus the weak electrons hopping than  $\text{Ni}_{0.9}\text{Mo}_{0.1}\text{-O}_x$  which cannot provide effective conductive pathways.

## pH Dependent CV & ETS Experiments

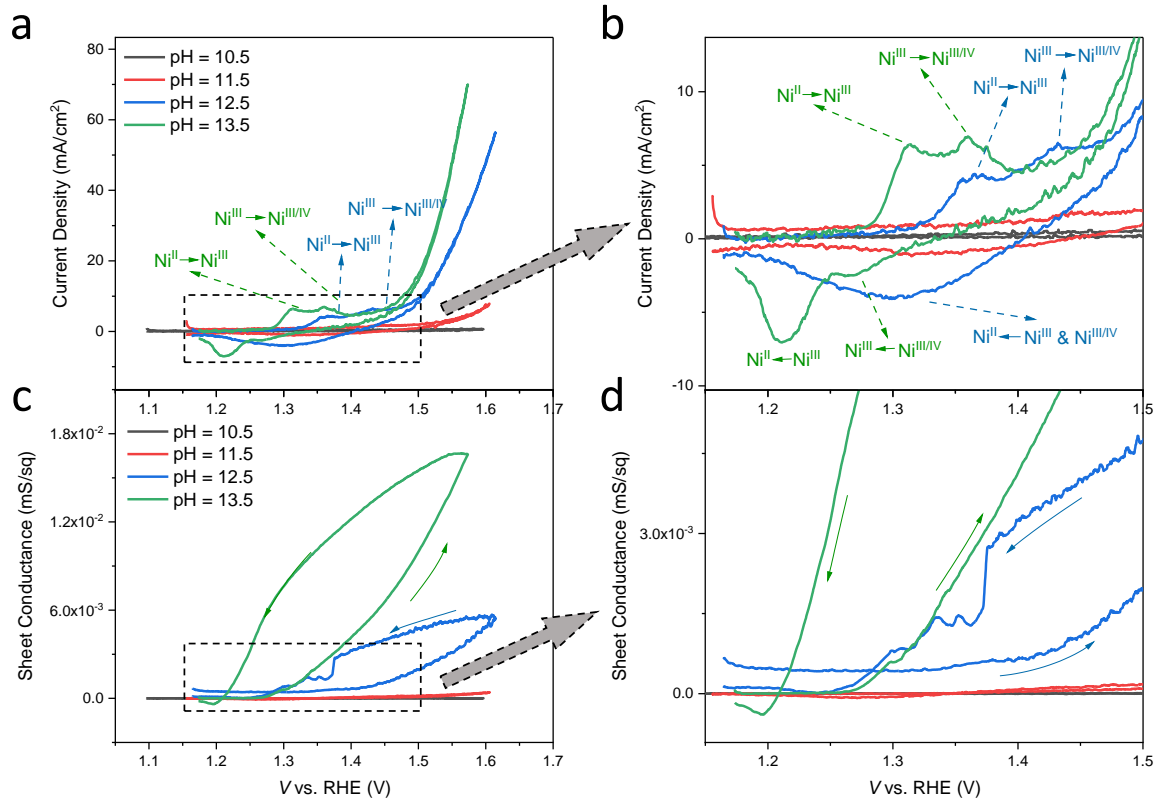


**Figure S41.** The pH dependent CV (**a, b**) & ETS (**c, d**) experiments of  $\alpha^*$ -Ni<sub>0.9</sub>Rh<sub>0.1</sub> devices in O<sub>2</sub>-saturated KOH (pH = 10.5–13.5) at a scan rate of 2 mV/s, the current density and sheet conductance have been normalized according to the shape of electrochemical window.

The results show that the OER activity of  $\gamma$ -Ni<sub>0.9</sub>Rh<sub>0.1</sub>OOH has a strong pH-dependence, better catalytic performance and the *in situ* conductance occur in electrolyte with higher pH values. This phenomenon can be rationalized that it is difficult for the transition metal ions to be oxidized to high oxidation states at near neutral pH and thus weak DE interaction (low *in situ* conductance) and large overpotential. While at relatively strong alkaline media, a large number of  $\gamma$ -Ni<sub>0.9</sub>Rh<sub>0.1</sub>OOH were generated at lower electrochemical potential to achieve enhanced DE interaction (higher *in situ* conductance) and better catalytic activity. These results support our idea that DE interaction induced transport properties in Ni-based oxyhydroxides can serve as an effective descriptor to reflect the oxidation states and d orbital occupancies of transition metal ions, which are crucial towards OER activity.

## Additional pDOS of other OER Intermediates

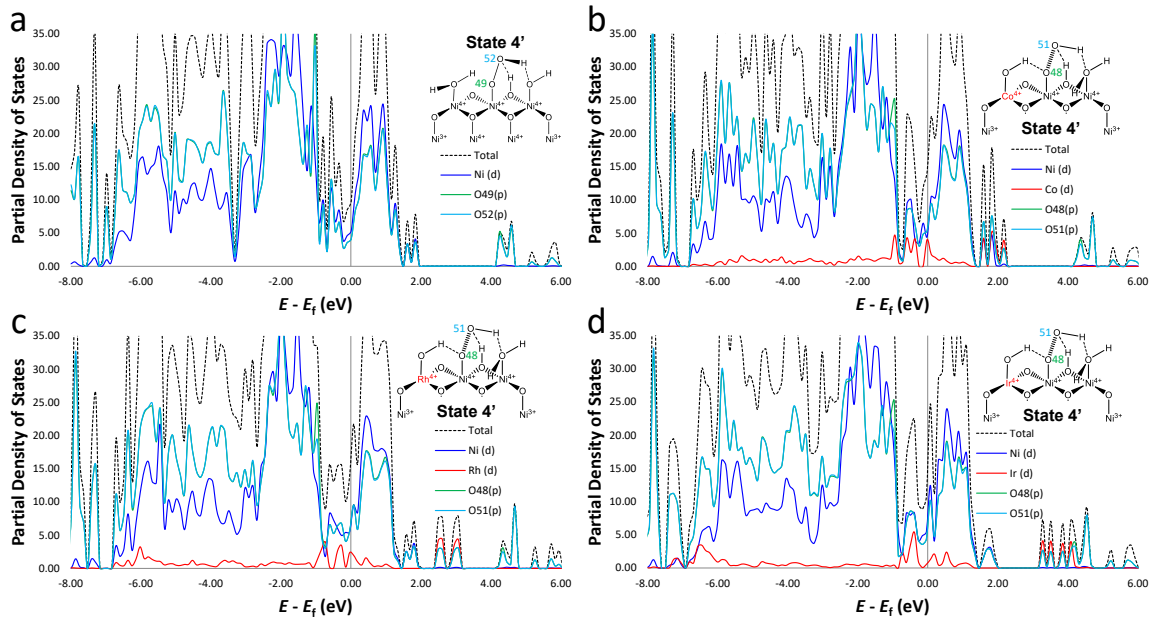


**Figure S42.** The partial Density of States of M-doped NiOOH-State 4' (solvation phase). The OER catalytic mechanism includes “State 4” intermediate as interpreted in detail in the literature.<sup>[19]</sup>

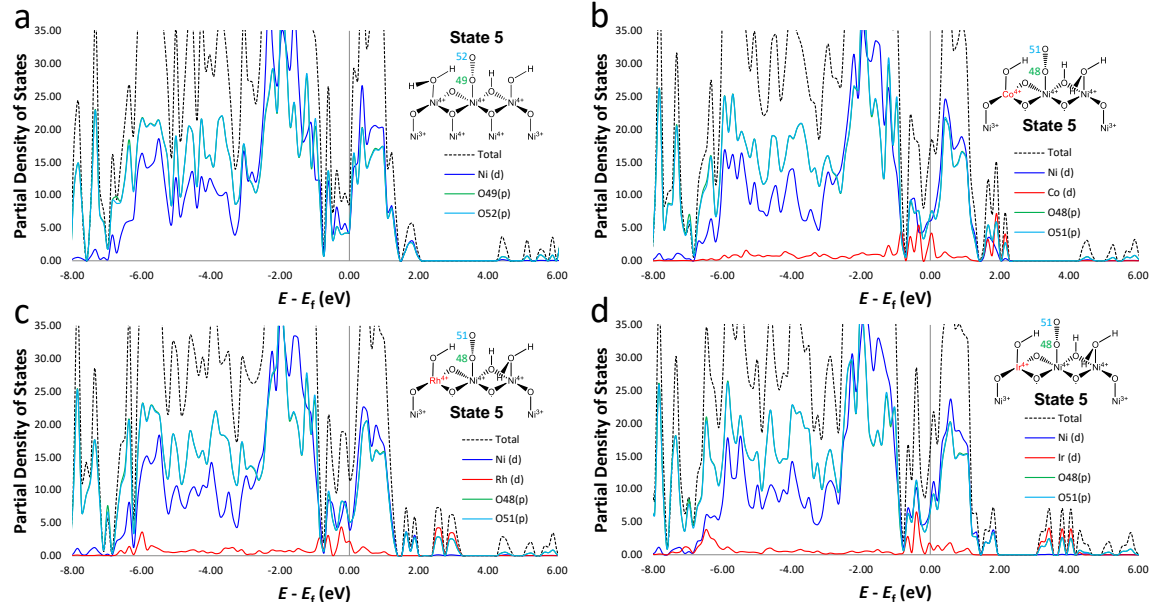


**Figure S43.** The partial Density of States of M-doped NiOOH-State 5 (solvation phase). The OER catalytic mechanism includes “State 5” intermediate as interpreted in detail in the literature.<sup>[19]</sup>

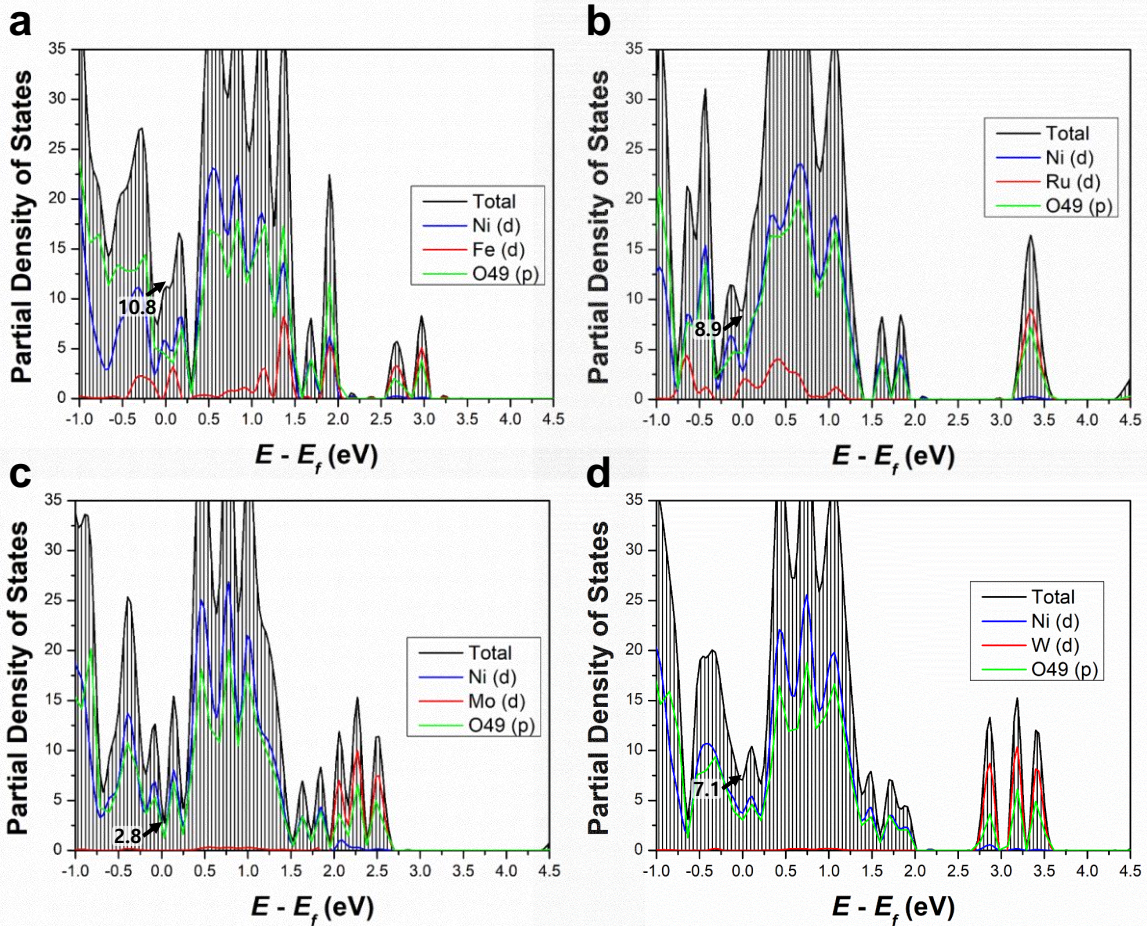


**Figure S44.** The partial Density of States of Fe, Ru, Mo and W doped  $\gamma$ -NiOOH-State 4 (solvation phase). Note that the State 4 of Ru, Mo and W doped  $\gamma$ -NiOOH do not exist due to different OER mechanism, as predicted in our previous theoretical calculations<sup>[19]</sup> and confirmed by our *in situ* conductivity measurements, while in Fe doped NiOOH there might be mixed/competing mechanisms as discussed in the main text.

As for Fe doped Ni hydroxide, we have carried out more systematic investigations on different samples from different synthetic approach. The mechanisms of  $\text{Ni}_{0.9}\text{Fe}_{0.1}$  LDHs are different with other metal doped Ni hydroxides, the similar conclusions are also drawn in ref<sup>[15-16]</sup>. The incorporation of Fe would change the OER active sites to Fe rather than Ni-Fe synergetic sites and thus the OER mechanisms. Since the DE interaction occurred in the system that M-O bonds have high covalency (high oxidation states) and the existence of  $\text{M}^{\text{IV}}=\text{O}^-$  species could be detected with higher *in situ* transport currents, in the system of Ni-Fe LDHs, the oxidation states of Ni won't be oxidized to  $\text{Ni}^{\text{III/IV}}$  and the nonexistence of  $\text{Fe}^{\text{IV}}=\text{O}^-$  together resulted in the relatively lower *in situ* conductivity (ref<sup>[16]</sup> reported that Fe remained at +3 state during OER). While the conductive intermediate phase (i.e., DE interactions) in  $\alpha^{\Delta}\text{-Ni}_{0.9}\text{Fe}_{0.1}(\text{OH})_2$  (prepared through ion-exchange) further confirms the Fe doping in the  $\alpha\text{-Ni}(\text{OH})_2$  can result in complicated consequences in terms of crystallinity, OER activity and mechanism. With proper synthetic approach,  $\alpha^{\Delta}\text{-Ni}_{0.9}\text{Fe}_{0.1}(\text{OH})_2$  (through ion-exchange in this study) showed expected improved OER activity and matching trend in activity-conductivity correlation. In all different cases, *in situ* conductivity was fundamentally determined by the high oxidation states on  $\text{Ni}^{\text{III/IV}}$  site (and consequently the higher degree of DE interaction), and its different characteristics can effectively reveal the different OER mechanisms. In the Mo and W doped NiOOH catalysts, it was also

reported that the incorporation of high valence Mo, W ( $\leq 10\%$ ) would change the oxidation behavior of Ni and Fe (making them remain at a low oxidation state during OER)<sup>[18]</sup>, and thus resulting in the very weak electrons hopping (DE) which cannot provide effective conductive pathways. Additionally, it can be more clearly noted in the Figure 4a that  $\alpha^{\star}\text{-Ni}_{0.9}\text{Ru}_{0.1}(\text{OH})_2$  and  $\alpha^{\Delta}\text{-Ni}_{0.9}\text{Fe}_{0.1}(\text{OH})_2$  show a slight shift to the linear correlation in Ir, Rh, Co, and pristine cases, which matched to the previous prediction that promotion of radical characters in metal-oxo bond mechanism exist in Ir, Rh, Co cases but not in Ru, Mo, and W cases. In Fe case, the mechanism is complicated, which may involve the combination/competition between two mechanistic pathways.

## Atomic Coordinates for All States in Figure 1a

### State 1

K Ni O H

1.0000000000000000	8.7372206091223994	0.0000000000000000	0.0000000000000000
0.0000000000000000	6.9809029500783426	0.0000000000000000	
0.0000000000000000	0.0000000000000000	25.0000000000000000	

K Ni O H  
4 12 35 22

Selective dynamics

Direct

0.0000000000000000	0.9295476953180497	0.0219900692777486
0.5000000000000000	0.8431778700801544	0.1149178963106294
0.0431977246227240	0.7582806340628593	0.2087123012227187
0.5427683855381095	0.6831659785942805	0.3448487673194416
0.0000000000000000	0.4295476953180497	0.0219900692777486
0.3336660000000009	0.4295476953180497	0.0219900692777486
0.6663339999999991	0.4295476953180497	0.0219900692777486
0.1663339999999991	0.3431778700801544	0.1149178963106294
0.5000000000000000	0.3431778700801544	0.1149178963106294
0.8336660000000009	0.3431778700801544	0.1149178963106294
0.9989226886732246	0.2558908428633444	0.2098439284415032
0.3333909255207630	0.2521053781339185	0.2103330282114551
0.6636181691821059	0.2545617767458928	0.2098836167092193
0.1644672719283788	0.1756692243982583	0.3061927389552984
0.5056543586010689	0.1766912594141325	0.3064125902023013
0.833750321368842	0.1881991365673761	0.3068311318022511
0.1735150000000019	0.5955569454815901	0.0004884286588833
0.5000000000000000	0.5859389052830437	0.0000000000000000
0.8264849999999981	0.5955569454815901	0.0004884286588833
0.1735150000000019	0.2635384451545022	0.0434917098966210
0.5000000000000000	0.2731564853530557	0.0439801385555043
0.8264849999999981	0.2635384451545022	0.0434917098966210
0.0000000000000000	0.4995690800451484	0.0929278270328737
0.3264849999999981	0.5091871202437019	0.0934162556917641
0.6735150000000019	0.5091871202437019	0.0934162556917641
0.0000000000000000	0.1867866601151604	0.1369079655883780
0.3264849999999981	0.1771686199166140	0.1364195369294947
0.6735150000000019	0.1771686199166140	0.1364195369294947
0.1676638371019280	0.4119173085264791	0.1883603227241292
0.4982952510549877	0.4154071566742359	0.1876686496997411
0.8267557542931614	0.4202263032629242	0.1879581390385082
0.1719262193808487	0.0947807067571802	0.2345672007256929
0.4977790296354649	0.0883671576564856	0.2281161991225893
0.8273854263778435	0.0977690102302338	0.2337976863263437
0.0048046144425974	0.3350677021648515	0.2808386216718469
0.3380364105504263	0.3286137742396575	0.2832969013456514
0.6611420516862356	0.3390923716122154	0.2819455892616711
0.9955684382783687	0.0237391676655541	0.3219818121419502
0.3381092565193691	0.0208540097858172	0.3330612362499552
0.6664739534257762	0.0419082395470131	0.3302702346613278
0.3436370000000011	0.9295476953180497	0.0219900692777486
0.6563629999999989	0.9295476953180497	0.0219900692777486
0.1563629999999989	0.8431778700801544	0.1149178963106294
0.8436370000000011	0.8431778700801544	0.1149178963106294
0.3571129455657219	0.7223767325332665	0.2493032945012214
0.7397980783313185	0.7233582491118192	0.2552773860670580
0.2026521474386872	0.6326919716892063	0.3531156277441717
0.8888194886288273	0.6961712836277725	0.3505540434099758
0.5627595155392418	0.3674051948835708	0.4097284503997190
0.8507552094006980	0.3039852228359534	0.3754290460540963
0.1521330182340190	0.2787721224346768	0.3781160529254926
0.2777910000000006	0.8194148176612188	0.0136009167645312
0.2777910000000006	0.0396805729748735	0.0303792217909731
0.7222089999999994	0.8194148176612188	0.0136009167645312
0.7222089999999994	0.0396805729748735	0.0303792217909731
0.2222089999999994	0.7330449924233307	0.1065287437974050
0.2222089999999994	0.9533107477369782	0.1233070488238468
0.7777910000000006	0.7330449924233307	0.1065287437974050
0.7777910000000006	0.9533107477369782	0.1233070488238468
0.4140891298453878	0.6218942671658899	0.2300737759814150
0.4100622623992318	0.8446501488363118	0.2422901520429057

0.7536438868808700 0.6302414848894883 0.2259355701101869  
 0.7550516233158341 0.8558049434589091 0.2420217083844661  
 0.2418980922620519 0.6464502371567944 0.3162961387896417  
 0.0921835441368550 0.6668742264951049 0.3506834040550604  
 0.8473264497661512 0.6936131347602904 0.3132784213554451  
 0.9155880640486866 0.8348560672251958 0.3544393412179374  
 0.6689524571059907 0.3183324875321217 0.4023097214000433  
 0.5364868118109675 0.3260611220510279 0.4456612295372047  
 0.0352733277019890 0.2765618194976200 0.3837820712199993  
 0.8602994955384563 0.4428699964458778 0.3679079177556165  
 0.3253146876836789 0.0519525071350344 0.3711242940687646  
 0.1804760979163698 0.4199648646274983 0.3710118736923418

## State 2

K Ni O H

1.0000000000000000		
8.7372206091223994	0.0000000000000000	0.0000000000000000
0.0000000000000000	6.9809029500783426	0.0000000000000000
0.0000000000000000	0.0000000000000000	25.0000000000000000

K Ni O H  
4 12 35 21

Selective dynamics

Direct

0.0000000000000000 0.9295476953180497 0.0219900692777486  
 0.5000000000000000 0.8431778700801544 0.1149178963106294  
 0.0219772289370202 0.7645102671146051 0.2073713123627349  
 0.5221860237024207 0.7074914228743956 0.3562244311306270  
 0.0000000000000000 0.4295476953180497 0.0219900692777486  
 0.3336660000000009 0.4295476953180497 0.0219900692777486  
 0.6663339999999991 0.4295476953180497 0.0219900692777486  
 0.1663339999999991 0.3431778700801544 0.1149178963106294  
 0.5000000000000000 0.3431778700801544 0.1149178963106294  
 0.8336660000000009 0.3431778700801544 0.1149178963106294  
 0.0012961495535132 0.2620747623372240 0.2100919939448649  
 0.3338739878040317 0.2579497279349519 0.2096999214961149  
 0.6665967355351463 0.2580840207787507 0.2092547305870878  
 0.1692939666191214 0.1784601680910908 0.3054598809790290  
 0.5046437118072188 0.1859296112248006 0.3044913510085394  
 0.8338643522243194 0.1858011288887492 0.3046234629882161  
 0.1735150000000019 0.5955569454815901 0.0004884286588833  
 0.5000000000000000 0.5859389052830437 0.0000000000000000  
 0.8264849999999981 0.5955569454815901 0.0004884286588833  
 0.1735150000000019 0.2635384451545022 0.0434917098966210  
 0.5000000000000000 0.2731564853530557 0.0439801385555043  
 0.8264849999999981 0.2635384451545022 0.0434917098966210  
 0.0000000000000000 0.4995690800451484 0.0929278270328737  
 0.3264849999999981 0.5091871202437019 0.0934162556917641  
 0.6735150000000019 0.5091871202437019 0.0934162556917641  
 0.0000000000000000 0.1867866601151604 0.1369079655883780  
 0.3264849999999981 0.1771686199166140 0.1364195369294947  
 0.6735150000000019 0.1771686199166140 0.1364195369294947  
 0.1691898666870562 0.4193368598413515 0.1872283079217001  
 0.4990383888845986 0.4179591577114631 0.1869559160197237  
 0.8314201037809903 0.4214325861611162 0.1876862891772020  
 0.1683850963046782 0.1036176290417214 0.2333250331638163  
 0.5010110505572180 0.0994218583626602 0.2317856189735233  
 0.8337261680986494 0.1009108481487715 0.2336718061959445  
 0.0028802184543310 0.3408240500934637 0.2823107898038140  
 0.3349628014351718 0.3385934139889731 0.2815515727703180  
 0.6678090491962858 0.3429302566166438 0.2802895864778854  
 -0.0021592566859802 0.0273369240582836 0.3237482699476721  
 0.3421390782394277 0.0260519612945379 0.3228947086425956  
 0.6690080069204597 0.0296909286814576 0.3219748085426093  
 0.3436370000000011 0.9295476953180497 0.0219900692777486  
 0.6563629999999989 0.9295476953180497 0.0219900692777486  
 0.1563629999999989 0.8431778700801544 0.1149178963106294  
 0.8436370000000011 0.8431778700801544 0.1149178963106294  
 0.2901826393955977 0.7251882265176370 0.2669960749061309  
 0.7141654161791503 0.7150389540771965 0.2614513232919779  
 0.1825117422473321 0.6223710212417533 0.3624652155136454  
 0.8682713130434493 0.6988584525810841 0.3556330376295847  
 0.5182659672882968 0.3068422705051227 0.3723098325429717  
 0.8163151471935557 0.3054410588638692 0.3770402317591246

0.1684447072865352	0.2711739846405071	0.3784379971340407
0.2777910000000006	0.8194148176612188	0.0136009167645312
0.2777910000000006	0.0396805729748735	0.0303792217909731
0.7222089999999994	0.8194148176612188	0.0136009167645312
0.7222089999999994	0.0396805729748735	0.0303792217909731
0.2222089999999994	0.7330449924233307	0.1065287437974050
0.2222089999999994	0.9533107477369782	0.1233070488238468
0.7777910000000006	0.7330449924233307	0.1065287437974050
0.7777910000000006	0.9533107477369782	0.1233070488238468
0.3726314824845948	0.6570393507124014	0.2488556776566294
0.3253505184986785	0.8568018478598782	0.2795440111555240
0.7279945610877649	0.6320055852380001	0.2301433118383743
0.7139521032122699	0.8511764672330664	0.2513609475065818
0.2196899398360929	0.6413781537120761	0.3245356696223293
0.0735271285430832	0.6618626574595257	0.3609291166444564
0.8279943920697254	0.6901643714460757	0.3182195853715611
0.9035997392944021	0.8349247769041508	0.3566509804665735
0.6988986682796208	0.2935056087785691	0.3821029963021381
0.4427988149647655	0.2382739471841590	0.3939507100517043
0.0659055658841757	0.2320616471057814	0.3903263075071554
0.8379162148170484	0.4446625946623879	0.3732111713853560
0.1717285424510631	0.4237205116770359	0.3734403385200936

## State 3

K Ni O H

1.000000000000000		
8.7372206091223994	0.0000000000000000	0.0000000000000000
0.0000000000000000	6.9809029500783426	0.0000000000000000
0.0000000000000000	0.0000000000000000	25.0000000000000000

K Ni O H

4 12 35 20

Selective dynamics

Direct

0.000000000000000	0.9295476953180497	0.0219900692777486
0.500000000000000	0.8431778700801544	0.1149178963106294
-0.002585876083442	0.7671346269876054	0.2119470605741065
0.4920874678869419	0.7640732935784272	0.3856704934546264
0.000000000000000	0.4295476953180497	0.0219900692777486
0.3336660000000009	0.4295476953180497	0.0219900692777486
0.6663339999999991	0.4295476953180497	0.0219900692777486
0.1663339999999991	0.3431778700801544	0.1149178963106294
0.500000000000000	0.3431778700801544	0.1149178963106294
0.8336660000000009	0.3431778700801544	0.1149178963106294
-0.002710542514955	0.2664242251192260	0.2105550443170425
0.3318709228674441	0.2625503705611819	0.2095105682130712
0.6668782861346676	0.2623483248058537	0.2093985312789806
0.1661233570552173	0.1923548437907445	0.3063502314410516
0.4991756696965112	0.1962064736730173	0.3042122038245993
0.8314622418367428	0.1941415200201544	0.3059162802322605
0.1735150000000019	0.5955569454815901	0.0004884286588833
0.500000000000000	0.5859389052830437	0.0000000000000000
0.8264849999999981	0.5955569454815901	0.0004884286588833
0.1735150000000019	0.2635384451545022	0.0434917098966210
0.500000000000000	0.2731564853530557	0.0439801385555043
0.8264849999999981	0.2635384451545022	0.0434917098966210
0.000000000000000	0.4995690800451484	0.0929278270328737
0.3264849999999981	0.5091871202437019	0.0934162556917641
0.67351500000000019	0.5091871202437019	0.0934162556917641
0.000000000000000	0.1867866601151604	0.1369079655883780
0.3264849999999981	0.1771686199166140	0.1364195369294947
0.67351500000000019	0.1771686199166140	0.1364195369294947
0.1657455472267081	0.4217053852494989	0.1868110967820061
0.4998948051353816	0.4175420070816093	0.1864626715182205
0.8329329850135335	0.4217956761275090	0.1867969138862821
0.1651470676477415	0.1109358209718709	0.2331212718091196
0.4995501047617127	0.1065232300780866	0.2315370564485392
0.8348664805196642	0.1106279392339288	0.2338981556319769
-0.001293298876153	0.3496783233081489	0.2824505514290350
0.3337092226391752	0.3514370133463907	0.2799479622847541
0.6639732730188800	0.3523323509055514	0.2796028938128073
-0.0010350201560570	0.0420585937432569	0.3243499714055292
0.3378549707099412	0.0370596833500826	0.3223480540523331
0.6611532199159101	0.0369697064513037	0.3224608903717315

0.3436370000000011 0.9295476953180497 0.0219900692777486  
 0.6563629999999989 0.9295476953180497 0.0219900692777486  
 0.1563629999999989 0.8431778700801544 0.1149178963106294  
 0.8436370000000011 0.8431778700801544 0.1149178963106294  
 0.2325312572812353 0.7173968892240560 0.2821801373228148  
 0.7663905695690288 0.7170265278813963 0.2843929167006110  
 0.1705189150324584 0.6652539137630783 0.3898423436505685  
 0.8554178212725873 0.6474939804032769 0.3849262588457468  
 0.5007987962219175 0.3142848060097598 0.3712980106064918  
 0.8110006115881979 0.2920218057158239 0.3774388099375114  
 0.1721586085826945 0.2848819081811843 0.3759695866751505  
 0.2777910000000006 0.8194148176612188 0.0136009167645312  
 0.2777910000000006 0.0396805729748735 0.0303792217909731  
 0.7222089999999994 0.8194148176612188 0.0136009167645312  
 0.7222089999999994 0.0396805729748735 0.0303792217909731  
 0.2222089999999994 0.7330449924233307 0.1065287437974050  
 0.2222089999999994 0.9533107477369782 0.1233070488238468  
 0.7777910000000006 0.7330449924233307 0.1065287437974050  
 0.7777910000000006 0.9533107477369782 0.1233070488238468  
 0.2965783907160089 0.6013467027510833 0.2788616344354599  
 0.2958515135278569 0.8353475238471346 0.2867317688793678  
 0.7008254492272276 0.6034235183613043 0.2789605384564540  
 0.7049456792019392 0.8371742778474196 0.2895165714773934  
 0.1760098750938847 0.7017414080696052 0.3513314948712162  
 0.1693710830475574 0.5217216293668411 0.3872328560480128  
 0.8378454048748837 0.6885509271366551 0.3467721183589199  
 0.9662821388976566 0.6743305918598087 0.3921084489399768  
 0.6977830392237657 0.2791440425873528 0.3836369357868094  
 0.3984225412429666 0.2798968939390092 0.3852321472302723  
 0.0900128992852268 0.2105284307955552 0.3928155015723335  
 0.8349618983279140 0.4415950876141634 0.3800265738487771

## State 4

K Ni O H  
 1.000000000000000  
 8.7372206091223994 0.000000000000000 0.000000000000000  
 0.000000000000000 6.9809029500783426 0.000000000000000  
 0.000000000000000 0.000000000000000 25.000000000000000

K Ni O H  
 4 12 36 21

Selective dynamics

Direct

0.000000000000000 0.9295476953180497 0.0219900692777486  
 0.500000000000000 0.8431778700801544 0.1149178963106294  
 -0.0003265507281078 0.7643873458160285 0.2128119121678972  
 0.4800858710527695 0.8097401443704785 0.3996833318649938  
 0.000000000000000 0.4295476953180497 0.0219900692777486  
 0.3336660000000009 0.4295476953180497 0.0219900692777486  
 0.6663339999999991 0.4295476953180497 0.0219900692777486  
 0.1663339999999991 0.3431778700801544 0.1149178963106294  
 0.500000000000000 0.3431778700801544 0.1149178963106294  
 0.8336660000000009 0.3431778700801544 0.1149178963106294  
 -0.0000293465417951 0.2644505302808114 0.2102589883507384  
 0.3322021799547887 0.2618777405007845 0.2098264673141764  
 0.6665506132320419 0.2603482198775274 0.2093063974170445  
 0.1651674973190403 0.1866694018668697 0.3061630999255814  
 0.5001928429840506 0.1936916196532949 0.3061867086191367  
 0.8324539410388943 0.1898070135187163 0.3051515404679754  
 0.1735150000000019 0.5955569454815901 0.0004884286588833  
 0.500000000000000 0.5859389052830437 0.000000000000000  
 0.8264849999999981 0.5955569454815901 0.0004884286588833  
 0.1735150000000019 0.2635384451545022 0.0434917098966210  
 0.500000000000000 0.2731564853530557 0.0439801385555043  
 0.8264849999999981 0.2635384451545022 0.0434917098966210  
 0.000000000000000 0.4995690800451484 0.0929278270328737  
 0.3264849999999981 0.5091871202437019 0.0934162556917641  
 0.6735150000000019 0.5091871202437019 0.0934162556917641  
 0.000000000000000 0.1867866601151604 0.1369079655883780  
 0.3264849999999981 0.1771686199166140 0.1364195369294947  
 0.6735150000000019 0.1771686199166140 0.1364195369294947  
 0.1656065395612832 0.4209779587497114 0.1869475135506296  
 0.4999599627105746 0.4166818876329703 0.1866132603371756  
 0.8333163342416410 0.4205071253592820 0.1868905353952071

0.1659466431042289	0.1092447484800991	0.2327848939005392
0.4988062222135731	0.1059626139297122	0.2316355037633262
0.8345934755714975	0.1073471149327922	0.2330451169426415
-0.0004678403223323	0.3454310199419155	0.2822275129895414
0.3328615695168772	0.3481839818194692	0.2808339427454397
0.6649734879355238	0.3484284147226218	0.2794889105114542
0.9977495953155020	0.0337957308576899	0.3222817908401970
0.3383540956772948	0.0336607407240575	0.3218482422744982
0.6630483392469790	0.0334401391968365	0.3229057913912161
0.3436370000000011	0.9295476953180497	0.0219900692777486
0.6563629999999989	0.9295476953180497	0.0219900692777486
0.1563629999999989	0.8431778700801544	0.1149178963106294
0.8436370000000011	0.8431778700801544	0.1149178963106294
0.2375694929974418	0.7128389681334321	0.2813875216154132
0.7657836444896026	0.7133610451006643	0.2851399418154140
0.1807487264059690	0.6539562753050535	0.3887191807639755
0.8676517525265348	0.6423905436746836	0.3846992022839820
0.5167753321359876	0.3134382924706147	0.3683147971265053
0.8164983215098778	0.2919349965366971	0.3759894787361632
0.1601621522079057	0.2688407443127265	0.3771619108330363
0.3548807548806081	0.1078553925833144	0.4477615452303266
0.2777910000000006	0.8194148176612188	0.0136009167645312
0.2777910000000006	0.0396805729748735	0.0303792217909731
0.7222089999999994	0.8194148176612188	0.0136009167645312
0.7222089999999994	0.0396805729748735	0.0303792217909731
0.2222089999999994	0.7330449924233307	0.1065287437974050
0.2222089999999994	0.9533107477369782	0.1233070488238468
0.7777910000000006	0.7330449924233307	0.1065287437974050
0.7777910000000006	0.9533107477369782	0.1233070488238468
0.3012659873754485	0.5958686932122884	0.2795717342124203
0.3020238661095760	0.8291717541560266	0.2863135935985009
0.6997627319390590	0.5994726850109228	0.2811806835152998
0.7032671454039959	0.8319265311824177	0.2910455196887091
0.1876622146331154	0.6893891365197030	0.3500925048177075
0.1796131285178355	0.5108063112188554	0.386781383325673
0.8441205160210088	0.6877460825664609	0.3474077730688528
0.9797916468309301	0.6670422545839867	0.3904307170023302
0.7000845382966719	0.2838423151084856	0.3809220420624476
0.0613740676147732	0.2149217919737786	0.3885781971803324
0.8444167799391566	0.4428898094221809	0.3786014285960417
0.3757936803987383	0.2093050693288025	0.4732864752613082
0.2866494768223371	0.1674293087583986	0.4197265701778259

## State 4'

K Ni O H

1.000000000000000		
8.7372206091223994	0.0000000000000000	0.0000000000000000
0.0000000000000000	6.9809029500783426	0.0000000000000000
0.0000000000000000	0.0000000000000000	25.0000000000000000

K Ni O H  
4 12 36 21

Selective dynamics

Direct

0.000000000000000	0.9295476953180497	0.0219900692777486
0.500000000000000	0.8431778700801544	0.1149178963106294
-0.0004377300953357	0.7665371236184298	0.2105854508263613
0.5474138491322136	0.7455687881253050	0.3923416178263027
0.000000000000000	0.4295476953180497	0.0219900692777486
0.3336660000000009	0.4295476953180497	0.0219900692777486
0.6663339999999991	0.4295476953180497	0.0219900692777486
0.1663339999999991	0.3431778700801544	0.1149178963106294
0.500000000000000	0.3431778700801544	0.1149178963106294
0.8336660000000009	0.3431778700801544	0.1149178963106294
-0.0004311046257435	0.2663482436415386	0.2098575367766323
0.3323796418749631	0.2619360737476999	0.2097581107551498
0.6668607301367893	0.2617701760985651	0.2091741604887839
0.1624911077017390	0.1922631825072682	0.3062358888968710
0.5049582479788398	0.1929044956033778	0.3049460059856989
0.8332306246869675	0.1920177598179424	0.3055177689980856
0.1735150000000019	0.5955569454815901	0.0004884286588833
0.5000000000000000	0.5859389052830437	0.0000000000000000
0.8264849999999981	0.5955569454815901	0.0004884286588833
0.1735150000000019	0.2635384451545022	0.0434917098966210

0.5000000000000000 0.2731564853530557 0.0439801385555043  
 0.826484999999981 0.2635384451545022 0.0434917098966210  
 0.0000000000000000 0.4995690800451484 0.0929278270328737  
 0.326484999999981 0.5091871202437019 0.0934162556917641  
 0.6735150000000019 0.5091871202437019 0.0934162556917641  
 0.0000000000000000 0.1867866601151604 0.1369079655883780  
 0.326484999999981 0.1771686199166140 0.1364195369294947  
 0.6735150000000019 0.1771686199166140 0.1364195369294947  
 0.1667657889765085 0.4220109993694590 0.1868783767633953  
 0.4993049858671654 0.4176933347908909 0.1865294009806717  
 0.8329722342571912 0.4211304375515060 0.1870198204801642  
 0.1646803494685877 0.1107418744382546 0.2335975568375116  
 0.4997236942709063 0.1049123082753331 0.2317709702404538  
 0.8345524612243584 0.1096407855119913 0.2338240862377764  
 0.997569534444125 0.3494809165621071 0.2817770916348182  
 0.3351674928797359 0.3469357180142081 0.2813905326470624  
 0.6629498860785070 0.3501389034144798 0.2806300119058811  
 0.9981757789328801 0.0398160034989905 0.3235740180505027  
 0.3448357445373841 0.0228612621213188 0.3251520060179487  
 0.6648341772769689 0.0332849774472825 0.3235729487273595  
 0.3436370000000011 0.9295476953180497 0.0219900692777486  
 0.6563629999999989 0.9295476953180497 0.0219900692777486  
 0.1563629999999989 0.8431778700801544 0.1149178963106294  
 0.8436370000000011 0.8431778700801544 0.1149178963106294  
 0.2224623445835508 0.7001169276216017 0.2861045722622884  
 0.7658096124988358 0.7144890916732284 0.2853595991938105  
 0.1823821364547148 0.6748907493794729 0.3940268183722132  
 0.8651132788675195 0.6559699102779009 0.3843585585731004  
 0.5131462216476700 0.3137231843323461 0.3743436326985284  
 0.8224052495732470 0.2942080385042066 0.3780861464421761  
 0.1655274168235713 0.2838865739371761 0.3783749632090315  
 0.4300323110106986 0.2128140636874085 0.4146834809179125  
 0.2777910000000006 0.8194148176612188 0.0136009167645312  
 0.2777910000000006 0.0396805729748735 0.0303792217909731  
 0.7222089999999994 0.8194148176612188 0.0136009167645312  
 0.7222089999999994 0.0396805729748735 0.0303792217909731  
 0.2222089999999994 0.7330449924233307 0.1065287437974050  
 0.2222089999999994 0.9533107477369782 0.1233070488238468  
 0.7777910000000006 0.7330449924233307 0.1065287437974050  
 0.7777910000000006 0.9533107477369782 0.1233070488238468  
 0.2821909356653481 0.5796307896171793 0.2818135451859923  
 0.293277710899658 0.8090995912442571 0.2888084670811694  
 0.6996126545233011 0.6025205545761321 0.2786140098671326  
 0.7054829963872281 0.8364436403470770 0.2894854979318623  
 0.1867780810768691 0.6983773525452239 0.3544786107847958  
 0.1769461729643742 0.5325974401798065 0.3943549031597496  
 0.8490137984995026 0.6920368459184347 0.3456427330094326  
 0.9742635045475670 0.6868905788049201 0.3926705445720761  
 0.7092446606014097 0.2832058929009340 0.3847393318735299  
 0.0751586739593916 0.2194863640645172 0.3932408966895415  
 0.8472889223546427 0.4406576855155719 0.3798568800360655  
 0.3414063387196568 0.0348420974940837 0.3644795107825679  
 0.3157041424711716 0.2505100011422038 0.4052567642998503

## State 5

K Ni O H

1.000000000000000  
 8.7372206091223994 0.0000000000000000 0.0000000000000000  
 0.0000000000000000 6.9809029500783426 0.0000000000000000  
 0.0000000000000000 0.0000000000000000 25.0000000000000000

K Ni O H  
4 12 36 20

Selective dynamics

Direct

0.000000000000000 0.9295476953180497 0.0219900692777486  
 0.500000000000000 0.8431778700801544 0.1149178963106294  
 0.9961659773456399 0.7655012177568289 0.2113959230288941  
 0.5229931894917942 0.7638198490621904 0.3938285379396821  
 0.000000000000000 0.4295476953180497 0.0219900692777486  
 0.3336660000000009 0.4295476953180497 0.0219900692777486  
 0.6663339999999991 0.4295476953180497 0.0219900692777486  
 0.1663339999999991 0.3431778700801544 0.1149178963106294  
 0.500000000000000 0.3431778700801544 0.1149178963106294

0.8336660000000009	0.3431778700801544	0.1149178963106294
0.0001103765821653	0.2638453458332449	0.2095918479337560
0.3330942807867945	0.2609138569007995	0.2095154451296117
0.6661739164349749	0.2608379191051171	0.2093422218011749
0.1615570838642056	0.1876702331827106	0.3049228789565738
0.5036386976537968	0.1958519959049570	0.3059153684456186
0.8343268207115717	0.1892709766443590	0.3054015009329699
0.1735150000000019	0.5955569454815901	0.0004884286588833
0.5000000000000000	0.5859389052830437	0.0000000000000000
0.826484999999981	0.5955569454815901	0.0004884286588833
0.1735150000000019	0.2635384451545022	0.0434917098966210
0.5000000000000000	0.2731564853530557	0.0439801385555043
0.826484999999981	0.2635384451545022	0.0434917098966210
0.0000000000000000	0.4995690800451484	0.0929278270328737
0.3264849999999981	0.5091871202437019	0.0934162556917641
0.6735150000000019	0.5091871202437019	0.0934162556917641
0.0000000000000000	0.1867866601151604	0.1369079655883780
0.3264849999999981	0.1771686199166140	0.1364195369294947
0.6735150000000019	0.1771686199166140	0.1364195369294947
0.1671524631360243	0.4209717523483316	0.1869470426237301
0.4993972323635512	0.4174069441729071	0.1866201603723611
0.8330295773508914	0.4198394679444681	0.1872748494491559
0.1668543146873144	0.1071364763541585	0.2325289373428577
0.4988852155241143	0.1028822786643025	0.2313278031012242
0.8325967355017949	0.1082006537858232	0.2337298429256991
0.0010014905503377	0.3444422193315810	0.2817654754735706
0.3348746414156488	0.3469605621835795	0.2809322426202909
0.6636266912429652	0.3496488083073174	0.2806261149829786
0.9980601760982211	0.0303625876975265	0.3204955375712085
0.3401846871149712	0.0345016326910342	0.3309245419273318
0.6640234774814704	0.0376679253129891	0.3249935288814750
0.3436370000000011	0.9295476953180497	0.0219900692777486
0.6563629999999989	0.9295476953180497	0.0219900692777486
0.1563629999999989	0.8431778700801544	0.1149178963106294
0.8436370000000011	0.8431778700801544	0.1149178963106294
0.2262867207143615	0.7026682897857541	0.2849514337149569
0.7652197462656244	0.7116048754416511	0.2903866168554922
0.1918257893069207	0.6524807341322846	0.3930840949903345
0.8689446776170778	0.6407735392636144	0.3874177463140046
0.5051428507750290	0.3287901415079888	0.3736041557973436
0.8426308794544474	0.2844310063941932	0.3787240737772771
0.1659386653119621	0.2668321895398668	0.3763038287382296
0.5448962659578567	0.2285300190581974	0.4157619589666053
0.2777910000000006	0.8194148176612188	0.0136009167645312
0.2777910000000006	0.0396805729748735	0.0303792217909731
0.7222089999999994	0.8194148176612188	0.0136009167645312
0.7222089999999994	0.0396805729748735	0.0303792217909731
0.2222089999999994	0.7330449924233307	0.1065287437974050
0.2222089999999994	0.9533107477369782	0.1233070488238468
0.7777910000000006	0.7330449924233307	0.1065287437974050
0.7777910000000006	0.9533107477369782	0.1233070488238468
0.2851399174456115	0.5820047441274545	0.2798663564359116
0.2968947557472137	0.8110634846865179	0.2865523054329942
0.6987018846508255	0.6007709668750466	0.2823818977319483
0.7063959519310745	0.8349889622042328	0.2936991660915796
0.1929411018835334	0.6858879117317970	0.3541990512735000
0.1899346093579414	0.5093861447375417	0.3913213795036150
0.8465907171164678	0.6816017367252369	0.3493211472000469
0.9797153150641394	0.6677797975495519	0.3939537059987890
0.7480388602868200	0.2401103355413346	0.3965943980506987
0.0653440391340271	0.2237894374002945	0.3893635890711898
0.8518256051430478	0.4367576989707015	0.3826239314193518
0.3083696870342585	0.0878429210093814	0.3665982542843826

## Atomic Coordinates for All States in Figure 1b (Fe)

### State 1

K Ni O H Fe

1.000000000000000  
8.7372206091223994 0.0000000000000000 0.0000000000000000  
0.0000000000000000 6.9809029500783426 0.0000000000000000  
0.0000000000000000 0.0000000000000000 25.0000000000000000

K Ni O H Fe

4 11 35 22 1

Selective dynamics

Direct

0.000000000000000 0.9295476953180497 0.0219900692777486  
0.500000000000000 0.8431778700801544 0.1149178963106294  
0.0456172516317765 0.7603924818685465 0.2074506794813830  
0.5409594686324396 0.6908385238927409 0.3379369486402265  
0.000000000000000 0.4295476953180497 0.0219900692777486  
0.3336660000000009 0.4295476953180497 0.0219900692777486  
0.6663339999999991 0.4295476953180497 0.0219900692777486  
0.1663339999999991 0.3431778700801544 0.1149178963106294  
0.500000000000000 0.3431778700801544 0.1149178963106294  
0.8336660000000009 0.3431778700801544 0.1149178963106294  
0.0001882631107049 0.2590405342296531 0.2098602570020885  
0.3330139409673090 0.2543032099467442 0.2101669821209445  
0.6634556167051613 0.2553271576283597 0.2098105677314869  
0.1628653062705149 0.1815269226551374 0.3066670008572200  
0.5049302662659991 0.1868140857707309 0.3083179885780539  
0.17351500000000019 0.5955569454815901 0.0004884286588833  
0.500000000000000 0.5859389052830437 0.0000000000000000  
0.8264849999999981 0.5955569454815901 0.0004884286588833  
0.17351500000000019 0.2635384451545022 0.0434917098966210  
0.500000000000000 0.2731564853530557 0.0439801385555043  
0.8264849999999981 0.2635384451545022 0.0434917098966210  
0.000000000000000 0.4995690800451484 0.0929278270328737  
0.3264849999999981 0.5091871202437019 0.0934162556917641  
0.67351500000000019 0.5091871202437019 0.0934162556917641  
0.000000000000000 0.1867866601151604 0.1369079655883780  
0.3264849999999981 0.1771686199166140 0.1364195369294947  
0.67351500000000019 0.1771686199166140 0.1364195369294947  
0.1691415743561835 0.4165385758065359 0.1876618681946938  
0.4971950471293527 0.4162219312889739 0.1874452701641842  
0.8295909391909274 0.4197182842871572 0.1880539414342748  
0.1687044353050434 0.0996391756759152 0.2330329395143918  
0.4971217234246310 0.0909371877151724 0.2288695555243115  
0.8294641043591722 0.1003274106840883 0.2342128816456880  
0.0042073263890282 0.3401867584932245 0.2812402995170368  
0.3372353138089630 0.3333952163447290 0.2828135283900369  
0.6617724430422767 0.3424816245229905 0.2810166708350539  
0.9896354329012630 0.0312415488339658 0.3247020776974170  
0.3356199361483611 0.0269525737305644 0.3331325721303772  
0.6724594733895295 0.0422913698601346 0.3287420024342198  
0.3436370000000011 0.9295476953180497 0.0219900692777486  
0.6563629999999989 0.9295476953180497 0.0219900692777486  
0.1563629999999989 0.8431778700801544 0.1149178963106294  
0.8436370000000011 0.8431778700801544 0.1149178963106294  
0.3593086604783626 0.7284501786891305 0.2459797046349141  
0.7435323058715448 0.7264219773380390 0.2527860344157993  
0.206412864577743 0.6369456084659251 0.3509498683876970  
0.8932251685906335 0.6942679094821449 0.3473955916427335  
0.5452677842436462 0.3481552297938087 0.3917465674599510  
0.8385076655179257 0.3203564344481081 0.3746415289969871  
0.1527714952653410 0.2885380817979053 0.3811919024235467  
0.2777910000000006 0.8194148176612188 0.0136009167645312  
0.2777910000000006 0.0396805729748735 0.0303792217909731  
0.7222089999999994 0.8194148176612188 0.0136009167645312  
0.7222089999999994 0.0396805729748735 0.0303792217909731  
0.2222089999999994 0.7330449924233307 0.1065287437974050  
0.2222089999999994 0.9533107477369782 0.1233070488238468  
0.7777910000000006 0.7330449924233307 0.1065287437974050  
0.7777910000000006 0.9533107477369782 0.1233070488238468  
0.4156259418892387 0.6276399836928521 0.2265313610870462  
0.4118405703378513 0.8515904092551209 0.2390856023752957  
0.7583474465021852 0.6303592925658109 0.2241472979562953  
0.7597015011408415 0.8579154220733991 0.2388256595337933

0.2446743803005780	0.6385993363377089	0.3138424433169881
0.0956757817179621	0.6686931118855554	0.3476327393943727
0.8505493405374949	0.6918198407760574	0.3102245774600376
0.9192803337042649	0.8332612639904678	0.3514054302173265
0.6613219097769089	0.3242574919205487	0.3913584147675148
0.5045596215486338	0.2905230825559570	0.4241697307703531
0.0392625451111155	0.2880181611791243	0.3877954844837160
0.8589206440206119	0.4572760507903416	0.3664901895153683
0.3199283990571293	0.0488170043838753	0.3714620280050874
0.1811415471151581	0.4282322340665290	0.3725557130144490
0.8334980958430774	0.1839499246661483	0.3082018969284069

## State 2

K Ni O H Fe

1.000000000000000		
8.7372206091223994	0.000000000000000	0.000000000000000
0.000000000000000	6.9809029500783426	0.000000000000000
0.000000000000000	0.000000000000000	25.000000000000000

K	Ni	O	H	Fe
4	11	35	21	1

Selective dynamics

Direct

0.000000000000000	0.9295476953180497	0.0219900692777486
0.500000000000000	0.8431778700801544	0.1149178963106294
0.0235833671848832	0.7610896156373953	0.2060604780785119
0.5169731789877821	0.7025250247669598	0.3559084647638948
0.000000000000000	0.4295476953180497	0.0219900692777486
0.3336660000000009	0.4295476953180497	0.0219900692777486
0.6663339999999991	0.4295476953180497	0.0219900692777486
0.1663339999999991	0.3431778700801544	0.1149178963106294
0.500000000000000	0.3431778700801544	0.1149178963106294
0.8336660000000009	0.3431778700801544	0.1149178963106294
0.0013214901205111	0.2601607355242959	0.2101236345407043
0.3335679120572116	0.2566583581952009	0.2097465313841758
0.6656605376723471	0.2554206745009699	0.2093906948664923
0.1675914118489314	0.1761576124255569	0.3061190896520535
0.5042509046903018	0.1839488092304573	0.3050782211915273
0.1735150000000019	0.5955569454815901	0.0004884286588833
0.5000000000000000	0.5859389052830437	0.0000000000000000
0.8264849999999981	0.5955569454815901	0.0004884286588833
0.1735150000000019	0.2635384451545022	0.0434917098966210
0.5000000000000000	0.2731564853530557	0.0439801385555043
0.8264849999999981	0.2635384451545022	0.0434917098966210
0.0000000000000000	0.4995690800451484	0.0929278270328737
0.3264849999999981	0.5091871202437019	0.0934162556917641
0.6735150000000019	0.5091871202437019	0.0934162556917641
0.0000000000000000	0.1867866601151604	0.136907965583780
0.3264849999999981	0.1771686199166140	0.1364195369294947
0.6735150000000019	0.1771686199166140	0.1364195369294947
0.1705263197099375	0.4197842669129754	0.1870616280080769
0.4983593844039415	0.4165474725039077	0.1871381683296095
0.8316037875144306	0.4184398777448762	0.1882232789532759
0.1676498120591235	0.1027597391300749	0.2325876086425917
0.5002654853694666	0.0972779614707206	0.2317165823166309
0.8314154699902981	0.0946834877826348	0.2336374102488543
0.0013210893465529	0.3358690036569651	0.2828523046984399
0.3354699137758174	0.3347727264821717	0.2816173252656241
0.6682356395428170	0.3387600885288264	0.2805558094752640
0.9892977107991894	0.0241681759341360	0.3258067765790533
0.3408412966624032	0.0250006440165839	0.3233195287794225
0.6728768568215672	0.0289074307152311	0.3249328644709922
0.3436370000000011	0.9295476953180497	0.0219900692777486
0.6563629999999989	0.9295476953180497	0.0219900692777486
0.1563629999999989	0.8431778700801544	0.1149178963106294
0.8436370000000011	0.8431778700801544	0.1149178963106294
0.2882160419188426	0.7235180003648963	0.2674844668763399
0.7118808673201048	0.7171872865743100	0.2590370651925053
0.1809129351504202	0.6236117531314204	0.3626695016546408
0.8598853990184218	0.6894075584384126	0.3544336575849882
0.5183996541328608	0.3073225857241580	0.3733362477652067
0.8147526331856771	0.3099840320492664	0.3771601909908951
0.1665579100468836	0.2706813820806821	0.3805331341816133
0.2777910000000006	0.8194148176612188	0.0136009167645312

0.2777910000000006 0.0396805729748735 0.0303792217909731  
 0.722208999999994 0.8194148176612188 0.0136009167645312  
 0.722208999999994 0.0396805729748735 0.0303792217909731  
 0.222208999999994 0.7330449924233307 0.1065287437974050  
 0.222208999999994 0.9533107477369782 0.1233070488238468  
 0.7777910000000006 0.7330449924233307 0.1065287437974050  
 0.7777910000000006 0.9533107477369782 0.1233070488238468  
 0.3694989510549683 0.6538625655215428 0.2491281741882700  
 0.3242769524446285 0.8549412455215030 0.2797256590959246  
 0.7280569250559341 0.6216626412821418 0.2306947213991578  
 0.7247800838674674 0.8469788219084714 0.2443563377769645  
 0.2176404748491191 0.6411841034706365 0.3246269994050054  
 0.0716060774433610 0.6588123612378232 0.3607915548868896  
 0.8201003039481086 0.6859021232388686 0.3168195973055712  
 0.8963178190612828 0.8241250070044970 0.3570622345735869  
 0.6970015745895752 0.3003777124361198 0.3827182655995697  
 0.4440721563692720 0.2388189253788066 0.3954325208998931  
 0.0635606429086364 0.2393375371797126 0.3934033707671934  
 0.8381155716407938 0.4486021688480463 0.3720225863804202  
 0.1722026452975610 0.4206726306163923 0.3751103880389295  
 0.8330159136527805 0.1706184616630597 0.3055510036950725

### State 3

K Ni O H Fe

1.000000000000000				
8.7372206091223994	0.000000000000000	0.000000000000000		
0.000000000000000	6.9809029500783426	0.000000000000000		
0.000000000000000	0.000000000000000	25.000000000000000		

K Ni O H Fe  
4 11 35 20 1

Selective dynamics

Direct

0.000000000000000 0.9295476953180497 0.0219900692777486  
 0.500000000000000 0.8431778700801544 0.1149178963106294  
 -0.0146916122734514 0.7637991030135463 0.2150514658032828  
 0.5695522313363484 0.7027411476933257 0.3599287341706607  
 0.000000000000000 0.4295476953180497 0.0219900692777486  
 0.3336660000000009 0.4295476953180497 0.0219900692777486  
 0.6663339999999991 0.4295476953180497 0.0219900692777486  
 0.1663339999999991 0.3431778700801544 0.1149178963106294  
 0.500000000000000 0.3431778700801544 0.1149178963106294  
 0.8336660000000009 0.3431778700801544 0.1149178963106294  
 0.0002150316937926 0.2652377656613481 0.2102207168140497  
 0.3320268592735747 0.2638813130185980 0.2099832341887780  
 0.6679477358076837 0.2630912485820907 0.2098184152149979  
 0.1636495566960492 0.1955145874867258 0.3069249466198768  
 0.5022013320818653 0.2015685296920332 0.3061175411488680  
 0.1735150000000019 0.5955569454815901 0.0004884286588833  
 0.500000000000000 0.5859389052830437 0.000000000000000  
 0.8264849999999981 0.5955569454815901 0.0004884286588833  
 0.1735150000000019 0.2635384451545022 0.0434917098966210  
 0.500000000000000 0.2731564853530557 0.0439801385555043  
 0.8264849999999981 0.2635384451545022 0.0434917098966210  
 0.000000000000000 0.4995690800451484 0.0929278270328737  
 0.3264849999999981 0.5091871202437019 0.0934162556917641  
 0.6735150000000019 0.5091871202437019 0.0934162556917641  
 0.000000000000000 0.186786601151604 0.1369079655883780  
 0.3264849999999981 0.1771686199166140 0.1364195369294947  
 0.6735150000000019 0.1771686199166140 0.1364195369294947  
 0.1666231120400849 0.4221376418737470 0.1869590429630182  
 0.4993990512409480 0.4192035435743851 0.1867976978359263  
 0.8337148328441522 0.4217135852309898 0.1867574751223445  
 0.166991704783033 0.1111942277236303 0.2338876136442866  
 0.4997214060112287 0.1092036233579269 0.2328740025021355  
 0.8338496179408927 0.1106226777239731 0.2329410907017381  
 -0.0002339012924240 0.3510812978342219 0.2811403514749847  
 0.3337348910639306 0.3541774362745931 0.280431711169258  
 0.6672691093766905 0.3537409878420632 0.2797252697940449  
 0.9868062241989306 0.0350738162700492 0.3238132058623439  
 0.3366981909638091 0.0477354106003138 0.3258546811814951  
 0.6716725420974088 0.0477828944682916 0.3257631223270521  
 0.3436370000000011 0.9295476953180497 0.0219900692777486  
 0.6563629999999989 0.9295476953180497 0.0219900692777486

0.1563629999999989 0.8431778700801544 0.1149178963106294  
 0.8436370000000011 0.8431778700801544 0.1149178963106294  
 0.2223748278043693 0.7195799264075785 0.2924252181982880  
 0.5986413342585424 0.7389224109250734 0.2479760487032575  
 0.2129680228817904 0.6442678930181568 0.3974469076902230  
 0.8883275969555103 0.7277274673675578 0.3914269131265964  
 0.5099207880313885 0.3198914969535283 0.3730986769809062  
 0.8334117497573571 0.3315903112216387 0.3709440367241829  
 0.1451689609579249 0.2888991615151777 0.3809837435313763  
 0.2777910000000006 0.8194148176612188 0.0136009167645312  
 0.2777910000000006 0.0396805729748735 0.0303792217909731  
 0.7222089999999994 0.8194148176612188 0.0136009167645312  
 0.7222089999999994 0.0396805729748735 0.0303792217909731  
 0.2222089999999994 0.7330449924233307 0.1065287437974050  
 0.2222089999999994 0.9533107477369782 0.1233070488238468  
 0.7777910000000006 0.7330449924233307 0.1065287437974050  
 0.7777910000000006 0.9533107477369782 0.1233070488238468  
 0.2864883511016142 0.6083912753134018 0.2825372034971648  
 0.2853865510818064 0.8394184277692954 0.2948345037800985  
 0.5491888651434245 0.6364786341916869 0.2272268234427269  
 0.5492961891912915 0.8621168660210530 0.2391913288549913  
 0.2093117625312526 0.6865044680015767 0.3588662459915325  
 0.1162794943908329 0.6945267617266658 0.4121183992461215  
 0.8882452080396459 0.5997392350475370 0.3746440198265442  
 0.9235641171536564 0.8221350162294581 0.3646292448818720  
 0.7297192189232391 0.3100358472823987 0.3860383260644960  
 0.4321373657069144 0.2501807708907224 0.3934970240582581  
 0.0327198915727584 0.2867756572952054 0.3876912325247631  
 0.1776569769695109 0.4300877381375622 0.3870606683406559  
 0.8324012363519289 0.1887562960057956 0.3083375963869681

## State 4

K Ni O H Fe  
 1.0000000000000000  
 8.7372206091223994 0.0000000000000000 0.0000000000000000  
 0.0000000000000000 6.9809029500783426 0.0000000000000000  
 0.0000000000000000 0.0000000000000000 25.0000000000000000

K Ni O H Fe  
 4 11 36 21 1

Selective dynamics

Direct

0.0000000000000000 0.9295476953180497 0.0219900692777486  
 0.5000000000000000 0.8431778700801544 0.1149178963106294  
 0.9810561718816594 0.7665505108314633 0.2132263917082290  
 0.5437097876716795 0.7532715337305980 0.3970406713408514  
 0.0000000000000000 0.4295476953180497 0.0219900692777486  
 0.3336660000000009 0.4295476953180497 0.0219900692777486  
 0.6663339999999991 0.4295476953180497 0.0219900692777486  
 0.1663339999999991 0.3431778700801544 0.1149178963106294  
 0.5000000000000000 0.3431778700801544 0.1149178963106294  
 0.8336660000000009 0.3431778700801544 0.1149178963106294  
 0.9989570327764271 0.2656214016395726 0.2102726462104375  
 0.3311984983106453 0.2628804541707555 0.2099898668514323  
 0.6672352501562534 0.2630345664806379 0.2098901794176269  
 0.1626592156717402 0.1943916926081247 0.3060743671683359  
 0.4998266427400375 0.2033036222231715 0.3061470662140889  
 0.1735150000000019 0.5955569454815901 0.0004884286588833  
 0.5000000000000000 0.5859389052830437 0.0000000000000000  
 0.8264849999999981 0.5955569454815901 0.0004884286588833  
 0.1735150000000019 0.2635384451545022 0.0434917098966210  
 0.5000000000000000 0.2731564853530557 0.0439801385555043  
 0.8264849999999981 0.2635384451545022 0.0434917098966210  
 0.0000000000000000 0.4995690800451484 0.0929278270328737  
 0.3264849999999981 0.5091871202437019 0.0934162556917641  
 0.6735150000000019 0.5091871202437019 0.0934162556917641  
 0.0000000000000000 0.1867866601151604 0.1369079655883780  
 0.3264849999999981 0.1771686199166140 0.1364195369294947  
 0.6735150000000019 0.1771686199166140 0.1364195369294947  
 0.1665509337734901 0.4219470621178407 0.1867575887754920  
 0.4973067367233813 0.4162780134924038 0.1869156074832171  
 0.8341107127112670 0.4203865259357460 0.1866227207562040  
 0.1651931669207395 0.1106887351950656 0.2343313855563812  
 0.4982112813872639 0.1102607203179267 0.2337321676946654

0.8330245208200164 0.1130826123810981 0.2326078035048271  
 0.9974979081295816 0.3529194009541952 0.2806086441393817  
 0.3303293525090423 0.3535711034153565 0.2811209884963613  
 0.6657147108060655 0.3571231497323984 0.2794927390839390  
 0.9894682189002425 0.0344320918128573 0.3218113458248258  
 0.3348642478278114 0.0447828993890028 0.3242380755067834  
 0.6667290438571934 0.0436224833327085 0.3237522866651032  
 0.3436370000000011 0.9295476953180497 0.0219900692777486  
 0.6563629999999989 0.9295476953180497 0.0219900692777486  
 0.1563629999999989 0.8431778700801544 0.1149178963106294  
 0.8436370000000011 0.8431778700801544 0.1149178963106294  
 0.2247241028075757 0.717856696331352 0.2909348162559784  
 0.6404539544864337 0.7622850908548313 0.2159855097653078  
 0.2075520714672231 0.6371490496758436 0.3951366199678385  
 0.8842590478270111 0.7197670274474655 0.3906283707277999  
 0.5097460964126754 0.3197082828278719 0.3731008316296531  
 0.8374759303504421 0.3278767666658081 0.3679532687211396  
 0.1430045764404770 0.2824498613421088 0.3790271353063638  
 0.4195521920316622 0.0528306588656853 0.4477085852695903  
 0.2777910000000006 0.8194148176612188 0.0136009167645312  
 0.2777910000000006 0.0396805729748735 0.0303792217909731  
 0.7222089999999994 0.8194148176612188 0.0136009167645312  
 0.7222089999999994 0.0396805729748735 0.0303792217909731  
 0.2222089999999994 0.7330449924233307 0.1065287437974050  
 0.2222089999999994 0.9533107477369782 0.1233070488238468  
 0.7777910000000006 0.7330449924233307 0.1065287437974050  
 0.7777910000000006 0.9533107477369782 0.1233070488238468  
 0.2893339195784263 0.6065744139810623 0.2817865474167817  
 0.2873769068436561 0.8381030040974253 0.2936704944444049  
 0.5925126208574608 0.6427451147253623 0.2275063294997489  
 0.5939562490561849 0.8657167711559839 0.2370196651941686  
 0.2080146699149137 0.6786499214057933 0.3563386643078931  
 0.1061240818676232 0.6808126556579638 0.4077471499360476  
 0.8743411862083631 0.5935812810430623 0.3728724415991748  
 0.9145102872644720 0.8141835008125223 0.3632320297950346  
 0.4461000659922282 0.1550464464654824 0.4212778460352202  
 0.0277962607579768 0.2924123707869622 0.3823823567216417  
 0.1813535854649554 0.4220961409396303 0.3853033311532358  
 0.6217301114170369 0.3159149238044864 0.3799696344881119  
 0.3083403494215963 0.0480389238689440 0.4455987503362017  
 0.8305968504485823 0.1946196129204482 0.3104545716530560

#### State 4'

K Ni O H Fe

1.000000000000000

8.7372206091223994 0.0000000000000000 0.0000000000000000  
 0.0000000000000000 6.9809029500783426 0.0000000000000000  
 0.0000000000000000 0.0000000000000000 25.0000000000000000

K Ni O H Fe

4 11 36 21 1

Selective dynamics

Direct

0.000000000000000 0.9295476953180497 0.0219900692777486  
 0.500000000000000 0.8431778700801544 0.1149178963106294  
 0.9882673081805069 0.7633688577663066 0.2097507022145051  
 0.6036238997352193 0.6759294211858190 0.3513119120352852  
 0.000000000000000 0.4295476953180497 0.0219900692777486  
 0.333666000000000 0.4295476953180497 0.0219900692777486  
 0.666333999999991 0.4295476953180497 0.0219900692777486  
 0.166333999999991 0.3431778700801544 0.1149178963106294  
 0.500000000000000 0.3431778700801544 0.1149178963106294  
 0.833666000000000 0.3431778700801544 0.1149178963106294  
 0.0018052882977446 0.2626032273260687 0.2096215766088663  
 0.3334023329266524 0.2591259255021907 0.2098231304688948  
 0.6694235906433273 0.2605563626260091 0.209688080141786  
 0.1634805974744891 0.1849082043911068 0.3060634832275422  
 0.5091917139318071 0.1890070345928628 0.3063723283785824  
 0.1735150000000019 0.5955569454815901 0.0004884286588833  
 0.500000000000000 0.5859389052830437 0.0000000000000000  
 0.8264849999999981 0.5955569454815901 0.0004884286588833  
 0.1735150000000019 0.2635384451545022 0.0434917098966210  
 0.500000000000000 0.2731564853530557 0.0439801385555043  
 0.8264849999999981 0.2635384451545022 0.0434917098966210  
 0.000000000000000 0.4995690800451484 0.0929278270328737  
 0.3264849999999981 0.5091871202437019 0.0934162556917641  
 0.6735150000000019 0.5091871202437019 0.0934162556917641

0.0000000000000000 0.1867866601151604 0.1369079655883780  
 0.3264849999999981 0.1771686199166140 0.1364195369294947  
 0.67351500000000019 0.1771686199166140 0.1364195369294947  
 0.1678480045256359 0.4204356913025482 0.1870550773916224  
 0.4990652625910704 0.4172662018619963 0.1870343232833228  
 0.8353076578726617 0.4196771600526228 0.1873129005348674  
 0.1678279032557842 0.1044634331426821 0.2328303157037404  
 0.5030520621479688 0.1021931708845414 0.2321822270269187  
 0.8362459728568236 0.1070460962563056 0.2332606475329962  
 0.0044362572684044 0.3441438933036653 0.2811554921591658  
 0.3363881094139226 0.3413917202294710 0.2815393013343868  
 0.6667010552735921 0.3464228760823493 0.2812923853778592  
 0.9922849088456647 0.0279228646939732 0.3233307702296488  
 0.3433158088254744 0.0211620427683478 0.3256787662916428  
 0.6789727373728294 0.0398079701095045 0.3263867246322492  
 0.3436370000000011 0.9295476953180497 0.0219900692777486  
 0.6563629999999989 0.9295476953180497 0.0219900692777486  
 0.1563629999999989 0.8431778700801544 0.1149178963106294  
 0.8436370000000011 0.8431778700801544 0.1149178963106294  
 0.2203986357325146 0.6942810605292733 0.2879798012985542  
 0.6106756754912503 0.7358475453499698 0.2435769932476090  
 0.2193672874834342 0.6402543208239748 0.3929064122432440  
 0.9082384623223092 0.7244242096152547 0.3904202370658001  
 0.5149949611675820 0.3054518869105255 0.3756112733967337  
 0.8483893800269287 0.3279162964483885 0.3712996037856246  
 0.1513083707533093 0.2861462553449561 0.3816863332685193  
 0.4451372366421666 0.1937970821264577 0.4167379771429414  
 0.2777910000000006 0.8194148176612188 0.0136009167645312  
 0.2777910000000006 0.0396805729748735 0.0303792217909731  
 0.7222089999999994 0.8194148176612188 0.0136009167645312  
 0.7222089999999994 0.0396805729748735 0.0303792217909731  
 0.2222089999999994 0.7330449924233307 0.1065287437974050  
 0.2222089999999994 0.9533107477369782 0.1233070488238468  
 0.7777910000000006 0.7330449924233307 0.1065287437974050  
 0.7777910000000006 0.9533107477369782 0.1233070488238468  
 0.2794770050447467 0.5754600461281304 0.2799426693887185  
 0.2899315323627471 0.8053289738996208 0.2885502299540511  
 0.5586347040628897 0.6348737419010473 0.2228553072063684  
 0.5626256812700768 0.8609399317083263 0.2356331193717824  
 0.2145477078058639 0.6722803698130907 0.3533652388969745  
 0.1205102437804303 0.6904282211311367 0.4064121610496148  
 0.9053869038015716 0.5957767826623199 0.3739952888870889  
 0.9382383949066235 0.8196358021171520 0.3628205218998205  
 0.3476436056929383 0.0168698898329438 0.3650867850305131  
 0.0373256683812834 0.2817052193034779 0.3882122734638469  
 0.1800055288113000 0.4314681154261726 0.3853197184613440  
 0.7547138654692322 0.2937802218567969 0.3908922067847296  
 0.3366731338976689 0.2389357076737733 0.4160212678064288  
 0.8378533674822164 0.1825980218410728 0.3075039130396380

## State 5

K Ni O H Fe

1.000000000000000  
 8.7372206091223994 0.0000000000000000 0.0000000000000000  
 0.0000000000000000 6.9809029500783426 0.0000000000000000  
 0.0000000000000000 0.0000000000000000 25.0000000000000000

K Ni O H Fe  
 4 11 36 20 1

Selective dynamics

Direct

0.000000000000000 0.9295476953180497 0.0219900692777486  
 0.500000000000000 0.8431778700801544 0.1149178963106294  
 0.9857444321261102 0.7634320715986770 0.2114316810784531  
 0.6092485568508154 0.6832337958494101 0.3518474616469796  
 0.000000000000000 0.4295476953180497 0.0219900692777486  
 0.3336660000000009 0.4295476953180497 0.0219900692777486  
 0.6663339999999991 0.4295476953180497 0.0219900692777486  
 0.1663339999999991 0.3431778700801544 0.1149178963106294  
 0.500000000000000 0.3431778700801544 0.1149178963106294  
 0.8336660000000009 0.3431778700801544 0.1149178963106294  
 0.9998817733660644 0.2628280076509055 0.2096278377181260  
 0.3313074227336404 0.2584036270978591 0.2098622998640508  
 0.6669186822294950 0.2606410833212151 0.2095748726413049

0.1607072028948470 0.1833057917815024 0.3062449584889774  
 0.5071155177701762 0.1889765160861706 0.3066174435171459  
 0.17351500000000019 0.5955569454815901 0.0004884286588833  
 0.5000000000000000 0.5859389052830437 0.0000000000000000  
 0.826484999999981 0.5955569454815901 0.0004884286588833  
 0.1735150000000019 0.2635384451545022 0.0434917098966210  
 0.5000000000000000 0.2731564853530557 0.0439801385555043  
 0.8264849999999981 0.2635384451545022 0.0434917098966210  
 0.0000000000000000 0.4995690800451484 0.0929278270328737  
 0.3264849999999981 0.5091871202437019 0.0934162556917641  
 0.6735150000000019 0.5091871202437019 0.0934162556917641  
 0.0000000000000000 0.1867866601151604 0.1369079655883780  
 0.3264849999999981 0.1771686199166140 0.1364195369294947  
 0.6735150000000019 0.1771686199166140 0.1364195369294947  
 0.1665087210642062 0.4201497692577152 0.1872148641659812  
 0.4980882247104562 0.4166444992779245 0.1873129073916197  
 0.8336162204855335 0.4202627561301256 0.1870585907963996  
 0.1646192345871748 0.1044597256543119 0.2322039983778454  
 0.5000502718431817 0.1010750053819366 0.2315033114219200  
 0.8329774765862643 0.1076353732740477 0.2329142642835800  
 0.9968715984965016 0.3484777257027003 0.2802141438966202  
 0.3328328481816189 0.3382016887949957 0.2816713556533973  
 0.6630553055696377 0.3482040152953090 0.2805514915899591  
 0.9885098596157874 0.0279087672936519 0.3223590903886427  
 0.3460230746060142 0.0188083683823314 0.3279780048058347  
 0.6775034218584595 0.0428475792992372 0.3271200218069797  
 0.3436370000000011 0.9295476953180497 0.0219900692777486  
 0.6563629999999989 0.9295476953180497 0.0219900692777486  
 0.1563629999999989 0.8431778700801544 0.1149178963106294  
 0.8436370000000011 0.8431778700801544 0.1149178963106294  
 0.2170795846648520 0.6949316155888429 0.2888254475951947  
 0.6105779360330140 0.7375513011490320 0.2431961405945169  
 0.2337902480159657 0.6368201922337512 0.3950946043559159  
 0.9111681900573719 0.7296567039035825 0.3916767694647711  
 0.5078229550502236 0.3102451124433598 0.3759298982440785  
 0.8480525074710418 0.3306292989509884 0.3711231480787335  
 0.1478514509877658 0.2745739871387189 0.3816130340308239  
 0.4946423277045554 0.2009714296407594 0.4170801333616143  
 0.2777910000000006 0.8194148176612188 0.0136009167645312  
 0.2777910000000006 0.0396805729748735 0.0303792217909731  
 0.7222089999999994 0.8194148176612188 0.0136009167645312  
 0.7222089999999994 0.0396805729748735 0.0303792217909731  
 0.2222089999999994 0.7330449924233307 0.1065287437974050  
 0.2222089999999994 0.9533107477369782 0.1233070488238468  
 0.7777910000000006 0.7330449924233307 0.1065287437974050  
 0.7777910000000006 0.9533107477369782 0.1233070488238468  
 0.2758321034747961 0.5766149890996753 0.2803799904467260  
 0.2875137464901121 0.8049843847279882 0.2912647384546041  
 0.5571076310328470 0.6345204622094913 0.2237991969409262  
 0.5589897907027238 0.8608675485589403 0.2357393212431491  
 0.2181563379906646 0.6665797336643695 0.3560383048323068  
 0.1397784819983969 0.6877435707863224 0.4115397759624868  
 0.9130029919655345 0.6009107126034229 0.3757144061006243  
 0.9441415452350503 0.8234972565464204 0.3641082429934809  
 0.3417559844656622 0.0173771364894207 0.3673145866600057  
 0.0332144224164553 0.2901762492711112 0.3851486839305525  
 0.1910478651683542 0.4081296957405738 0.3879000938388386  
 0.7857930463943281 0.2667906084774587 0.3982136459079292  
 0.8355375169717228 0.1849106462755564 0.3069580794318858

## Supplementary References

- [1] M. Gao, W. Sheng, Z. Zhuang, Q. Fang, S. Gu, J. Jiang, Y. Yan, *J. Am. Chem. Soc.* **2014**, *136*, 7077-7084.
- [2] a) U. Halim, C. R. Zheng, Y. Chen, Z. Lin, S. Jiang, R. Cheng, Y. Huang, X. Duan, *Nat. Commun.* **2013**, *4*, 1-7; b) Z. Mu, M. Yang, W. He, Y. Pan, P. Zhang, X. Li, X. Wu, M. Ding, *J. Phys. Chem. Lett.* **2020**, *11*, 5798-5806.
- [3] J. P. Perdew, K. Burke, M. Ernzerhof, *Phys. Rev. Lett.* **1996**, *77*, 3865-3868.
- [4] G. Kresse, J. Furthmüller, *Phys. Rev. B* **1996**, *54*, 11169-11186.
- [5] G. Kresse, D. Joubert, *Phys. Rev. B* **1999**, *59*, 1758.
- [6] B. Wang, K. Zhao, Z. Yu, C. Sun, Z. Wang, N. Feng, L. Mai, Y. Wang, Y. Xia, *Energy Environ. Sci.* **2020**, *13*, 2200-2208.
- [7] X. Zheng, B. Zhang, P. De Luna, Y. Liang, R. Comin, O. Voznyy, L. Han, F. P. García de Arquer, M. Liu, C. T. Dinh, T. Regier, J. J. Dynes, S. He, H. L. Xin, H. Peng, D. Prendergast, X. Du, E. H. Sargent, *Nat. Chem.* **2018**, *10*, 149-154.
- [8] F. Dionigi, Z. Zeng, I. Sinev, T. Merzdorf, S. Deshpande, M. B. Lopez, S. Kunze, I. Zegkinoglou, H. Sarodnik, D. Fan, A. Bergmann, J. Drnec, J. F. d. Araujo, M. Gliech, D. Teschner, J. Zhu, W.-X. Li, J. Greeley, B. R. Cuenya, P. Strasser, *Nat. Commun.* **2020**, *11*, 2522.
- [9] Q. Zhou, Y. Chen, G. Zhao, Y. Lin, Z. Yu, X. Xu, X. Wang, H. K. Liu, W. Sun, S. X. Dou, *ACS Catal.* **2018**, *8*, 5382-5390.
- [10] a) M. J. Natan, D. Belanger, M. K. Carpenter, M. S. Wrighton, *J. Phys. Chem.* **1987**, *91*, 1834-1842; b) L. Trotochaud, S. L. Young, J. K. Ranney, S. W. Boettcher, *J. Am. Chem. Soc.* **2014**, *136*, 6744-6753.
- [11] a) M. Ding, Q. He, G. Wang, H.-C. Cheng, Y. Huang, X. Duan, *Nat. Commun.* **2015**, *6*, 1-9; b) M. Ding, G. Zhong, Z. Zhao, Z. Huang, M. Li, H.-Y. Shiu, Y. Liu, I. Shakir, Y. Huang, X. Duan, *ACS Cent. Sci.* **2018**, *4*, 590-599.
- [12] J. Huang, Y. Li, Y. Zhang, G. Rao, C. Wu, Y. Hu, X. Wang, R. Lu, Y. Li, J. Xiong, *Angew. Chem. Int. Ed.* **2019**, *58*, 17458-17464.
- [13] Z. Xiao, Y.-C. Huang, C.-L. Dong, C. Xie, Z. Liu, S. Du, W. Chen, D. Yan, L. Tao, Z. Shu, G. Zhang, H. Duan, Y. Wang, Y. Zou, R. Chen, S. Wang, *J. Am. Chem. Soc.* **2020**, *142*, 12087-12095.
- [14] M. S. Burke, L. J. Enman, A. S. Batchellor, S. Zou, S. W. Boettcher, *Chem. Mater.* **2015**, *27*, 7549-7558.
- [15] S. Lee, K. Banjac, M. Lingenfelder, X. Hu, *Angew. Chem. Int. Ed.* **2019**, *58*, 10295-10299.
- [16] M. Görlin, P. Chernev, J. Ferreira de Araújo, T. Reier, S. Dresp, B. Paul, R. Krähnert, H. Dau, P. Strasser, *J. Am. Chem. Soc.* **2016**, *138*, 5603-5614.
- [17] M. F. Liu, Z. Z. Du, Y. L. Xie, X. Li, Z. B. Yan, J. M. Liu, *Sci. Rep.* **2015**, *5*, 9922.
- [18] a) B. Zhang, L. Wang, Z. Cao, S. M. Kozlov, F. P. García de Arquer, C. T. Dinh, J. Li, Z. Wang, X. Zheng, L. Zhang, Y. Wen, O. Voznyy, R. Comin, P. De Luna, T. Regier, W. Bi, E. E. Alp, C.-W. Pao, L. Zheng, Y. Hu, Y. Ji, Y. Li, Y. Zhang, L. Cavallo, H. Peng, E. H. Sargent, *Nat. Catal.* **2020**, *3*, 985-992; b) L. Wang, Y. Zhu, Y. Wen, S. Li, C. Cui, F. Ni, Y. Liu, H. Lin, Y. Li, H. Peng, B. Zhang, *Angew. Chem. Int. Ed.* **2021**, *n/a*.
- [19] H. Shin, H. Xiao, W. A. Goddard III, *J. Am. Chem. Soc.* **2018**, *140*, 6745-6748.